Anisotropy in granular media: Classical elasticity and directed-force chain network

M. Otto,[1] J.-P. Bouchaud,[2] P. Claudin,[3] and J. E. S. Socolar[4]
[1] *Institut für Theoretische Physik, Universität Göttingen, Bunsenstrasse 9, D-37075 Göttingen, Germany*
[2] *Service de Physique de l'Etat Condensé, CEA-Saclay, Orme des Merisiers, 91191 Gif-sur-Yvette Cedex, France*
[3] *Laboratoire des Milieux Désordonnés et Hétérogènes (UMR 7603), 4 place Jussieu, Case 86, 75252 Paris Cedex 05, France*
[4] *Department of Physics and Center for Nonlinear and Complex Systems, Duke University, Durham, North Carolina 27708*
(Received 1 November 2002; revised manuscript received 23 December 2002; published 25 March 2003)

A general approach is presented for understanding the stress response function in anisotropic granular layers in two dimensions. The formalism accommodates both classical anisotropic elasticity theory and linear theories of anisotropic directed-force chain networks. Perhaps surprisingly, two-peak response functions can occur even for classical, anisotropic elastic materials, such as triangular networks of springs with different stiffnesses. In such cases, the peak widths grow linearly with the height of the layer, contrary to the diffusive spreading found in "stress-only" hyperbolic models. In principle, directed-force chain networks can exhibit the two-peak, diffusively spreading response function of hyperbolic models, but all models in a particular class studied here are found to be in the elliptic regime.

DOI: 10.1103/PhysRevE.67.031302 PACS number(s): 45.70.Cc, 83.80.Fg

I. INTRODUCTION

The stress response of an assembly of hard, cohesionless grains has been a subject of debate [1–4]. The dividing line has been mostly between traditional approaches based on elasticity or elastoplasticity theory on one hand, and "stress-only" models on the other which make no reference to a local deformation field but posit (history-dependent) closure relations between components of the stress tensor. The former leads to elliptic partial differential equations for the stresses, for which boundary conditions must be imposed everywhere on the boundary. In contrast, the latter approach often leads to hyperbolic equations [3,4]. The wavelike behavior of their solutions has been at the origin of a proposed physical mechanism called stress propagation through the bulk granular material. In an infinite slab geometry, it only requires the specification of boundary conditions on the "top" surface. A family of (linear) closure relations have been shown to account for the pressure dip underneath the apex of a sandpile and stresses in silos [3,4]. Alternative explanations based on elastoplasticity are found in Ref. [5].

The phenomenological stress-only closure relations follow from plausible symmetry arguments, and can be seen as the coarse-grained version of local probabilistic rules for stress transfer [6]. However, these relations lack a detailed microscopic derivation that would allow one to understand both their range of validity and to compute the phenomenological parameters from the statistical properties of the packing, except in the case of frictionless grains. In fact, a system of frictionless polydisperse spheres is shown to be isostatic [7–10], i.e., the number of unknown forces is equal to the number of equations for mechanical equilibrium. If an isostatic system is sufficiently anisotropic, a linear closure relation between stresses can be derived [11]. Further attempts to obtain the missing equation for stresses from a microscopic approach for different packings are presented in [11,12], but these are still somewhat inconclusive. In particular, in the case of a completely isotropic packing, none of the homogeneous linear closure relations is compatible with the rotational symmetry. The idea of "grains" (in the metallurgical sense) and packing defects must be introduced to restore the large scale symmetry.

In order to understand stress distribution on a more fundamental level, we have introduced the mesoscopic concept of the directed-force chain network (DFCN) [13,14], which is motivated by the experimental evidence for filamentary force chains in a wide variety of systems [15]. The "double Y" model has been developed to describe such networks based on simple rules for the splitting and merging of straight force chains. This model leads to a nonlinear Boltzmann equation for the probability $P(f,\hat{\mathbf{n}},\mathbf{r})$ of finding a force chain at the spatial point $\mathbf{r}$ with intensity f in the direction $\hat{\mathbf{n}}$.

In the first paper [13], chain merging (which produces the nonlinear terms in the Boltzmann equation) was neglected. An isotropic splitting rule was assumed, corresponding to strongly disordered isotropic granular packings. A pseudoelastic theory for the stress tensor was derived in which the role of the displacement field is played by a vector field $\mathbf{J}(\mathbf{r})=\langle\hat{\mathbf{n}}f\rangle$ that represents the coarse-grained or ensemble averaged force chain direction. A relation between $\partial_i J_j$ and the stress tensor exists that is formally equivalent to an isotropic stress-strain relation. The resulting elliptic equations yield a response function with a unique (pseudoelastic) peak, as observed experimentally in strongly disordered packings [16,17]. Further study showed, however, that the nonlinear terms in the Boltzmann equation contain essential physics and cannot be neglected [14]. In fact, for an exactly solvable model with six discrete directions for force chains, it was found that the elliptic (pseudoelastic) behavior of the response function is limited to small depths, and that at sufficiently large depths a crossover occurs to a hyperbolic response, i.e., two Gaussian peaks that propagate away and broaden diffusively. Whether this behavior is specific to the model with six discrete directions is a subject of current study, and the elliptic or hyperbolic nature of the linearized response around the full solution of the nonlinear Boltzmann equation is an open question.

Following a different route, Goldenberg and Goldhirsch [18] have recently noted that a two-peak response function can be found in classical anisotropic ball-and-spring models. Gay and da Silveira [19] have furthermore given some arguments for the relevance of anisotropic elasticity for the large scale description of granular assemblies of compressible grains that can locally rotate. The two-peak nature of the response function is therefore not in itself a signature of hyperbolicity, but may occur in elliptic systems that are sufficiently anisotropic. The unambiguous signature of hyperbolic response lies in the scaling of the peak widths with depth, which is linear in generic elliptic systems but diffusive (proportional to the square root of depth) in generic hyperbolic systems. In the linear pseudoelasticity theories discussed below, the diffusive spreading in hyperbolic systems is not captured; the peaks appear as δ functions that do not spread at all. Deviations from elasticity on small scales and their possible relation with granular media were also discussed in Ref. [20].

The aim of this paper is to give a unified account of the shape of the response function for anisotropic systems described either by standard elasticity theory or the pseudoelastic theory that emerges from an approximate linear treatment of directed-force networks. Though there are open questions concerning the self-consistency of the latter, there do appear to be some contexts in which the equations of the pseudoelasticity theory hold, and they may be especially relevant for systems of intermediate depth (large compared to the disorder length scale but not much larger than the persistence length of force chains).

Very recently, the response functions of two-dimensional (2D) granular layers subjected to shear have been determined experimentally [27]. Under shear, an anisotropic texture appears and force chains are preferably oriented along an angle of 45°. Within the (pseudo)elasticity framework presented below, this provides motivation for studying materials characterized by a selected global direction **N**.

The paper is organized as follows. In Sec. II, a general mathematical framework for calculating stress response functions in anisotropic materials. The main results of the paper are then summarized in a "phase diagram" indicating where "one-peak" or "two-peak" response functions can appear in parameter space. In Sec. III, we compute the analytic form of the response function for the various phases and show a number of examples for the variety of shapes that are possible, including a brief comment on relation to experimental work. In Sec. IV, we show how the formalism applies to the example of a triangular ball-and-spring network, indicating how spring stiffnesses must be chosen to access all possible regions of the general parameter space. In Sec. V, a linear anisotropic pseudoelastic theory is derived from an anisotropic linear directed-force chain network model and it is shown that this class of models always lies in the elliptic regime. A conclusion is given in Sec. VI. Algebraic details of several calculations are presented in the Appendixes.

II. ANISOTROPIC ELASTICITY AND SUMMARY OF OUR RESULTS

A. General equations for 2D systems with arbitrary anisotropy

In the following, we present a general framework that covers both classical linear anisotropic elasticity theory [21] and a generally anisotropic "pseudoelasticity" theory, that appears within a linearized treatment of directed-force chain networks (see Sec. V). The large scale equations that can be derived in these two approaches are formally identical, although the "pseudostrain" has a geometric meaning different from the usual strain tensor. For simplicity, we will restrict the discussion to two-dimensional systems.

The most general linear relation between the stress tensor $\boldsymbol{\sigma}$ and a symmetric tensor formed from the gradients of a vector field $\mathbf{u}$ is

$$\sigma_{ij}=\lambda_{ijkl}u_{kl}\,, \tag{1}$$

where σ_{ij} denotes a component of the stress tensor, $u_{ij} \equiv \frac{1}{2}(\partial_j u_i+\partial_i u_j)$, and summation over repeated indices is implied. In the classical linear theory of elasticity, the vector u_i is the displacement field describing the physical deformation of a continuous medium. For usual elastic bodies, the antisymmetric combination $\partial_j u_i-\partial_i u_j$ corresponds to a local rotation of the material, which is not allowed here. For granular materials, on the other hand, grains might locally rotate due to the presence of friction. This extension which suggests a continuum description in terms of Cosserat elasticity was recently discussed in Ref. [19]. The absence of internal torques requires that the stress tensor is also symmetric. The coefficients λ_{ijkl} are material constants and form the elastic modulus tensor. The indices i,j,k,l are equal to x,z, where for later purposes x is to be considered as the horizontal coordinate and z a vertical coordinate pointing downward.

Symmetry of both the stress and the strain tensor imply a permutation symmetry within the first and second pair of indices for λ_{ijkl}, i.e.,

$$\lambda_{ijkl}=\lambda_{jikl}=\lambda_{ijlk}=\lambda_{jilk}\,. \tag{2}$$

Materials whose behavior is modeled only in terms of Eq. (1) without any reference to a free energy functional are characterized by an elastic modulus tensor that need not have any symmetries other than Eq. (2). They are called "hypoelastic" when u_{ij} corresponds to a real strain tensor [22]. In hyperelastic materials, on the other hand, the existence of quadratic free energy functional,

$$F=\frac{1}{2}\lambda_{ijkl}u_{ij}u_{kl}\,, \tag{3}$$

gives an additional symmetry under exchange of the first and second pair of indices, i.e.,

$$\lambda_{ijkl}=\lambda_{klij}\,. \tag{4}$$

In the "pseudoelasticity" theory, the vector u_i will be a novel geometric quantity (see below), and the resulting tensor u_{ij} will be called a pseudoelastic strain tensor. This tensor is still symmetric, as explained in Sec. V, but the above additional symmetry is, in general, *not* present.

We wish to construct general solutions of the equilibrium equations

$$\partial_i \sigma_{ij} = 0. \tag{5}$$

In order to close the problem for the stress tensor, a supplementary condition is needed which is the condition of compatibility,

$$\partial_z^2 u_{xx} + \partial_x^2 u_{zz} - 2\partial_x \partial_z u_{xz} = 0, \tag{6}$$

resulting simply from the fact that the tensor u_{ij} is built with the derivatives of a vector u_i. This relation does not depend on a specific interpretation of the tensor in terms of real deformations.

The entries of the stress and strain tensors can be arranged in vector form, i.e., $\mathbf{\Sigma} = (\sigma_{xx}, \sigma_{zz}, \sigma_{xz})^T$ and $\mathbf{U} = (u_{xx}, u_{zz}, u_{xz})^T$, giving a matrix representation of the elastic modulus tensor,

$$\mathbf{\Sigma} = \Lambda \mathbf{U}, \tag{7}$$

where

$$\Lambda = \begin{pmatrix} \lambda_{xxxx} & \lambda_{xxzz} & 2\lambda_{xxxz} \\ \lambda_{zzxx} & \lambda_{zzzz} & 2\lambda_{zzxz} \\ \lambda_{xzxx} & \lambda_{xzzz} & 2\lambda_{xzxz} \end{pmatrix}. \tag{8}$$

The factors of 2 are due to the symmetry under exchange of the last two indices of λ_{ijkl} and u_{kl}. Now, we want to express the compatibility relation in terms of the stress tensor, so we need to express $\mathbf{U}$ in terms of $\mathbf{\Sigma}$, i.e.,

$$\mathbf{U} = \mathcal{B} \mathbf{\Sigma}, \tag{9}$$

where $\mathcal{B} = (B_{ij}) = \Lambda^{-1}$. Then Eq. (6) for an anisotropic medium is rewritten as follows:

$$B_{1j} \partial_z^2 \Sigma_j + B_{2j} \partial_x^2 \Sigma_j - 2B_{3j} \partial_x \partial_z \Sigma_j = 0. \tag{10}$$

For an isotropic medium, $B_{11} = B_{22}$, $B_{21} = B_{12}$, $B_{3i} = B_{i3} = 0$, for $i = 1,2$, thus the equation reduces to $\Delta(\sigma_{xx} + \sigma_{zz}) = 0$.

In the following, we will look for solutions of the form $\sigma_{ij} \propto e^{iqx + i\omega z}$. In this case, Eq. (10), together with the conditions of mechanical equilibrium (5), can be rewritten in matrix form,

$$\boldsymbol{\mathcal{A}}(q,\omega)\mathbf{\Sigma} = 0. \tag{11}$$

A nontrivial solution occurs if $\det(\boldsymbol{\mathcal{A}}(q,\omega)) = 0$, which leads to a certain *dispersion relation* of the form $\omega(q) = Xq$, where X obeys the following equation:

$$\frac{B_{22}}{B_{11}} - \frac{B_{23} + 2B_{32}}{B_{11}} X + \frac{2B_{33} + B_{21} + B_{12}}{B_{11}} X^2 - \frac{B_{13} + 2B_{31}}{B_{11}} X^3 + X^4 = 0. \tag{12}$$

Depending on whether the roots X are real or complex, the response function will be qualitatively different.

(a) Complex roots, corresponding to elliptic equations for the stress, appear within the classical theory of anisotropic elasticity. The fact that the roots are complex follows from the positivity of the free energy [23].

(b) Purely real roots can occur in the context of directed-force chain networks considered below. The existence of at least one purely real root of the dispersion relation classifies the problem at hand as hyperbolic [23].

B. The case of uniaxial symmetry

Let us consider the case of uniaxial anisotropy and choose x and z to be along the principal axes of anisotropy. Then only λ_{ijkl} with even numbers of equal indices is nonzero. Due to the symmetry (2) of λ_{ijkl}, this leaves one, in general, with five different constants. The matrix Λ takes the form

$$\Lambda_\dagger = \begin{pmatrix} a & c & 0 \\ c' & b & 0 \\ 0 & 0 & d \end{pmatrix}. \tag{13}$$

We denote it with a dagger to indicate that it corresponds to a material with a vertical uniaxial symmetry. An alternative parametrization of $\Lambda_\dagger$, standard in elasticity theory, is

$$\Lambda_\dagger = \frac{1}{1 - \nu_x \nu_z} \begin{pmatrix} E_x & \nu_z E_x & 0 \\ \nu_x E_z & E_z & 0 \\ 0 & 0 & (1 - \nu_x \nu_z) G \end{pmatrix}, \tag{14}$$

where $E_{x,z}$ and G are the Young and shear moduli, respectively, and $\nu_{x,z}$ the Poisson ratios. Note that the present form includes a linear elasticity theory without a free energy functional. The classical theory is recovered with the extra symmetry $c' = c$. In this case, E_x, E_z, ν_x, and ν_z are not independent, satisfying the relation $E_z / E_x = \nu_z / \nu_x$. Together with G, we are thus left with four independent constants.

In classical elasticity theory for a uniaxial system, the stress-strain relation is derivable from an energy density of the form

$$F = \frac{1}{2}[a u_{xx}^2 + b u_{zz}^2 + 2c u_{xx} u_{zz} + 2d u_{xz}^2]. \tag{15}$$

The material described is stable under deformations if and only if F is positive definite for any strain, which requires

$$a > 0, \quad b > 0, \quad d > 0, \quad \text{and} \quad ab - c^2 > 0. \tag{16}$$

Or, equivalently,

$$\nu_x \nu_z < 1, \quad E_x > 0, \quad E_z > 0, \quad \text{and} \quad G > 0. \tag{17}$$

An elastic material that is permitted to reversibly deform must obey these constraints, but they do not apply to materials for which there is no well-defined free energy quadratic in the strains. We speak of such materials as being described by coefficients that lie outside the ''classical stability'' range.

The compatibility condition (6) expressed in terms of the stress tensor reads

$$b\partial_z^2\sigma_{xx}-c\partial_z^2\sigma_{zz}-c'\partial_x^2\sigma_{xx}+a\partial_x^2\sigma_{zz}-2\frac{\det\Lambda}{d^2}\partial_x\partial_z\sigma_{xz}=0. \tag{18}$$

Combining this relation with the two equilibrium conditions of Eq. (5),

$$\partial_z\sigma_{zz}+\partial_x\sigma_{xz}=0, \tag{19}$$

$$\partial_z\sigma_{xz}+\partial_x\sigma_{xx}=0, \tag{20}$$

we obtain, for any one of the components of the stress tensor,

$$(\partial_z^4+t\partial_x^4+2r\partial_x^2\partial_z^2)\sigma_{ij}=0, \tag{21}$$

where the coefficients t and r are given by

$$t=\frac{a}{b}=\frac{E_x}{E_z},$$

$$r=\frac{ab-cc'-\frac{1}{2}d(c+c')}{bd}=\frac{1}{2}E_x\left(\frac{2}{G}-\frac{\nu_z}{E_z}-\frac{\nu_x}{E_x}\right). \tag{22}$$

Expanding the stresses in Fourier modes, it is easy to see that the solutions of the Eqs. (19)–(21) are of the form

$$\sigma_{zz}=\int_{-\infty}^{+\infty}dq\sum_k a_k(q)e^{iqx+iX_kqz}, \tag{23}$$

$$\sigma_{xz}=C_{xz}-\int_{-\infty}^{+\infty}dq\sum_k a_k(q)X_ke^{iqx+iX_kqz}, \tag{24}$$

$$\sigma_{xx}=C_{xx}+\int_{-\infty}^{+\infty}dq\sum_k a_k(q)X_k^2e^{iqx+iX_kqz}, \tag{25}$$

where C_{xx} and C_{xz} are constants. From Eq. (21), we see that the X_k are the roots of the following quartic equation:

$$X^4+2rX^2+t=0, \tag{26}$$

a special case of Eq. (12). There are four solutions

$$X=\pm\sqrt{-r\pm(r^2-t)^{1/2}}. \tag{27}$$

Hence the index k runs from 1 to 4. The four functions $a_k(q)$ and the constants C_{xx} and C_{xz} must be determined by the boundary conditions, as shown in Sec. III and Appendix B.

We see that only two combinations, r and t, of the five elastic constants will determine the structure of the response function in anisotropic materials.

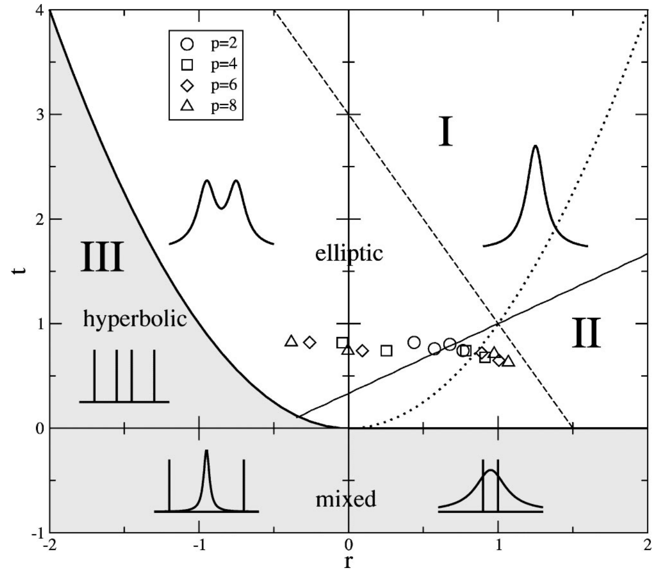

FIG. 1. (r,t) phase diagram characterizing the qualitative nature of the stress profiles. The shaded region corresponds to hyperbolic and ''mixed'' equations for stresses, whereas the unshaded region allows for elliptic equations. The hyperbolic region is bounded above by the line $t=r^2$, separating it from the elliptic region. In the elliptic region, a double-peak stress profile is found in the whole region $r<0$. The solid and dashed straight lines are the trajectories for the triangular spring network studied in Sec. IV, for horizontal and vertical orientation of one of the springs, respectively. The symbols correspond to the solutions of the anisotropic linear DFCN model for various values of the anisotropic scattering parameter p; see Sec. V.

C. Main results of this paper

We show in Fig. 1 the various ''phases'' in the r-t plane corresponding to different shapes of the response function, as obtained from the calculation presented in Sec. III below.

The line $t=r^2$, for $r<0$, separates the hyperbolic and the elliptic regions. For $t>r^2$ (region I), the above roots X_k are complex and we write

$$X_1=-X_4=\beta-i\alpha, \tag{28}$$

$$X_2=-X_3=-\beta-i\alpha, \tag{29}$$

where α and β are positive real numbers. When $t<r^2$, $r>0$ (region II), one the other hand, the roots X_k are purely imaginary and one has

$$X_1=-X_4=-i\alpha_1, \tag{30}$$

$$X_2=-X_3=-i\alpha_2, \tag{31}$$

where α_1 and α_2 are positive real numbers.

Note that the isotropic limit corresponds to the point $r=1, t=1$. As we show in detail in Sec. III, the elliptic region contains a subregion $r<0$, $t>r^2$, where the response function has a two-peak structure with peak widths growing linearly with depth. As one approaches the line $t=r^2$, the two peaks become narrower and narrower, finally becoming two δ-function peaks exactly on the transition line. Below the transition, there is a hyperbolic regime (region III in Fig. 1), where the response consists of four δ-function peaks.

The parameter range $t<0$, labeled ''mixed'' in Fig. 1, gives rise to a third type of behavior of the response function due to the fact that there are two real roots and two imaginary roots. It may only appear in the nonstable pseudoelastic case, and gives superposition of a hyperbolic two δ peak response function and a single-peak classically elastic response function. For the particular model for the DFCN discussed below, the range $t<0$ does not occur. Hence, this case is not pursued any further here.

We discuss below some particular trajectories in the r-t plane (see Secs. IV and V). One corresponds to simple, anisotropic, triangular networks of springs, that lead on large scales to classical anisotropic elasticity with parameters on the plain and dotted straight lines, corresponding to two orientations of the lattice (see Fig. 10). Both trajectories meet at the point (1,1) corresponding to an isotropic medium where all springs have the same stiffness. Moreover, both trajectories cross the region $r<0$ and thus allow for two-peak response functions. Inclusion of three-body forces permits spring networks with (r,t) anywhere in region I or II (see Sec. IV).

We have also computed r and t for the linear DFCN model, for a particular model for scattering where the degree of anisotropy is tuned in terms of a parameter p (see Sec. V). The results are shown as symbols, and appear to always lie in the elliptic region. As in the spring networks, for sufficiently anisotropic scattering, one enters the region $r<0$ where the response function has two peaks.

In two classical papers [24], Green *et al.* have treated the stress distribution inside plates with two directions of symmetry with right angles to each other. The solutions are parametrized, apart from boundary conditions, by α_1,α_2 (not to be confused with α_i introduced above), which are related to the set r,t by $(r+\sqrt{r^2-t}/t),(r-\sqrt{r^2-t}/t)$. The authors assume their parameters α_1,α_2 to be always real and positive, based on empirical fits of elastic constants for timbers such as oak and spruce. This choice corresponds to region II in Fig. 1. Consequently, the possibility of regions I and III behavior, and particularly the appearance of a double-peak response for a classically elastic material, is not discussed in [24]. Moreover, their analysis considers the response in the case where the boundaries and the directions of symmetry are either parallel or perpendicular to each other, whereas the present discussion—see, in particular Sec. III B—treats a more general case. The response functions for region II, as computed in the present work, could, in principle, be reconstructed from the results of Ref. [24].

III. SHAPE OF THE RESPONSE FUNCTION

After having discussed the general framework of anisotropic elasticity and the particular example of two-dimensional systems with uniaxial symmetry, we now turn to the actual shape of the response function in such materials. We will calculate the response of an elastic or pseudoelastic slab of infinite horizontal extent to a localized force applied at the top surface. We shall consider the case of a semi-infinite system with a force applied at a single point on its surface, for which complete analytical solutions can be obtained. More general situations (finite spatial extension of the overload, finite thickness of the slab with a rough or smooth bottom, . . .) should be considered to obtain quantitative fits of experimental [16,17] and numerical data. Still, two angles are left free: the angle θ_0 that the applied force makes with the vertical, and the orientation angle τ of the anisotropy with the vertical.

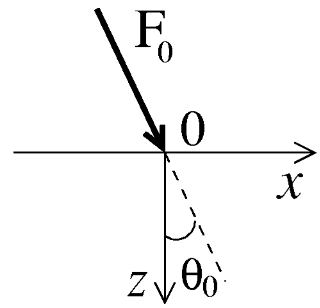

FIG. 2. Force at the top surface.

A. Vertical anisotropy

We are interested in the response of a semi-infinite system to a localized force at its top surface $z=0$. We suppose that this force is of amplitude F_0 and makes an angle θ_0 with the vertical direction, as shown in Fig. 2. The corresponding stresses at $z=0$ are then

$$\sigma_{zz}=F_0\cos\theta_0\,\delta(x), \tag{32}$$

$$\sigma_{xz}=F_0\sin\theta_0\,\delta(x). \tag{33}$$

To obtain the results described below, we make use of the identity

$$\delta(x)=\frac{1}{2\pi}\int_0^{+\infty}dq\,(e^{iqx}+e^{-iqx}), \tag{34}$$

and impose the boundary condition by identifying the coefficients of $e^{\pm iqx}$ in the Eqs. (32) and (33), and (23)–(25) at $z=0$. Note that $\sigma_{xx}(z=0)$ is not determined by the boundary conditions.

When $z\to+\infty$, we expect all stresses to decay to zero. It turns out that this is a self-consistent condition as long as the system is energetically stable, but cannot be imposed in the unstable regime. The reader interested in a more detailed derivation of the following results can consult Appendix B.

1. Region I (elliptic): $t>r^2$

Since we want all the stresses to vanish at large depth, the functions a_1 and a_2 in Eqs. (23)–(25) must be zero for $q>0$, and a_3 and a_4 must vanish for $q<0$. In addition, C_{xx} and C_{xz} must all vanish. Furthermore, because the stresses are real quantities, $a_1(-q)=a_3^*(q)$ and $a_2(-q)=a_4^*(q)$.

The boundary conditions at $z=0$ then imply

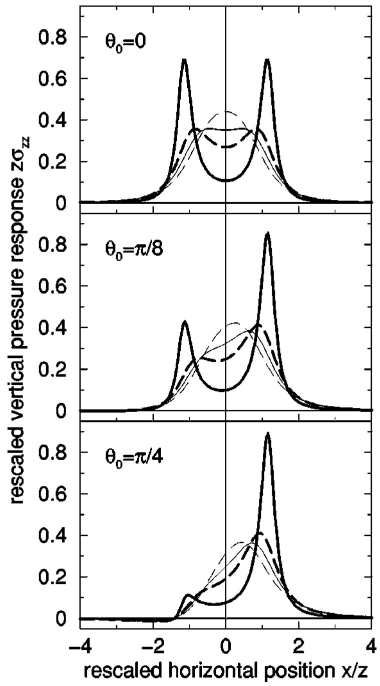

FIG. 3. *Region I*: rescaled stress profiles for several directions θ_0 of the applied force and several values of r, with $t=2$. In each panel, the thick solid line is for $r=-1.3$, the thick dashed line is for $r=-0.7$, the thin solid line is for $r=-0.2$, and the thin dashed line is for $r=0.5$. $r>0$ is the condition to have a single-peaked profile for $\theta_0=0$.

$$a_3=\frac{F_0}{4\pi\beta}[(\beta-i\alpha)\cos\theta_0-\sin\theta_0], \tag{35}$$

$$a_4=\frac{F_0}{4\pi\beta}[(\beta+i\alpha)\cos\theta_0+\sin\theta_0]. \tag{36}$$

Since the coefficients a_3 and a_4 are independent of q, the integrals in Eqs. (23)–(25) are straightforwardly carried out, yielding

$$\sigma_{zz}=\frac{F_0}{2\pi}\,\frac{4\alpha z^2[z\cos\theta_0(\alpha^2+\beta^2)+x\sin\theta_0]}{[(\alpha^2-\beta^2)z^2+x^2]^2+[2\alpha\beta z^2]^2}, \tag{37}$$

$$\sigma_{xz}=\frac{x}{z}\sigma_{zz}, \tag{38}$$

$$\sigma_{xx}=\left(\frac{x}{z}\right)^2\sigma_{zz}. \tag{39}$$

The latter two results follow directly from the observation that the integrals in Eqs. (24) and (25) can be expressed simply as convolutions of $\sigma_{zz}(q)$ with the Fourier transforms of x/z and x^2/z^2, respectively. In the limit $\beta\to 0$ (which corresponds to $r^2-t\to 0$) and $\alpha\to 1$, we recover the familiar isotropic formulas [21].

Figure 3 shows the response for four different choices of the parameter r and a fixed t, each being shown for three choices of θ_0. Note that σ_{zz} has a more pronounced double-peak structure for increasingly negative r. For $\theta_0=0$, the condition for having a double peak is $\partial_x^2\sigma_{zz}(x=0)>0$, which occurs when $\alpha^2<\beta^2$, or equivalently $r<0$. In terms of the Young and shear moduli and the Poisson ratios, this condition can be expressed as $G>E_x/\nu_x=E_z/\nu_z$. The positions of the peaks are then given by $x=\pm z\sqrt{\beta^2-\alpha^2}=\pm z\sqrt{|r|}$. From the curvature at the maximum, one can define a width w of these peaks which reads

$$w=\frac{\alpha\beta}{\sqrt{2}}\,\frac{1}{\sqrt{\beta^2-\alpha^2}}z=\frac{\sqrt{t-r^2}}{2\sqrt{2|r|}}z. \tag{40}$$

Thus, the peaks become sharper and sharper as one approaches the hyperbolic limit $t=r^2$.

A very important point is that the response profiles scale with the reduced variable x/z when multiplied by the height z. This means that, when the profile is double peaked, these two peaks get larger in the same way that they get away from each other. Such a response cannot therefore be seen as an "hyperboliclike" signature, for which the peak width compared to the distance between the peaks goes to zero at large depth. However, in the limit where $t\to r^2$, the width of the peak vanishes, and the response becomes truly hyperbolic.

2. Region II (elliptic): $t<r^2$, $r>0$

Again, we only keep the functions a_1 and a_2 for $q<0$, and a_3 and a_4 for $q>0$. This time, the fact that stresses are real quantities requires $a_1^*(-q)=a_4(q)$ and $a_2^*(-q)=a_3(q)$. A similar analysis to the above yields

$$\sigma_{zz}=\frac{F_0}{2\pi}\,\frac{2(\alpha_1+\alpha_2)z^2[\alpha_1\alpha_2 z\cos\theta_0+x\sin\theta_0]}{[(\alpha_1 z)^2+x^2][(\alpha_2 z)^2+x^2]}, \tag{41}$$

$$\sigma_{xz}=\frac{x}{z}\sigma_{zz}, \tag{42}$$

$$\sigma_{xx}=\left(\frac{x}{z}\right)^2\sigma_{zz}. \tag{43}$$

For $\alpha_1=\alpha_2=1$ (again $r^2-t=0$), we recover the isotropic formula. In this case, however, when $\theta_0=0$, σ_{zz} always presents a single peak, see Fig. 4. Depending on the values of α_1 and α_2, the profiles can be broader or narrower than the isotropic response, as has been observed experimentally on, respectively, dense and loose packings [16].

3. Region III (hyperbolic): $t<r^2$, $r<0$

In this case, all the roots X_k are real, and the response function is the sum of four δ peaks, at positions $x=X_k z$. The appearance of four peaks is different from previous hyperbolic models [3,4] giving two peaks in which case the closure relation for the stresses is linear, whereas here the closure is achieved by a fourth-order partial differential equation, Eq. (21). The four peaks merge into two peaks exactly on the hyperbolic-elliptic boundary $t=r^2$. The reason why previous hyperbolic models [3,4] work so well could be that granular system such as sandpiles are close to

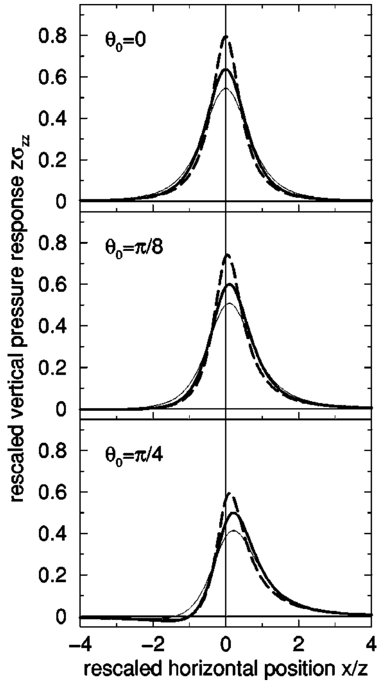

FIG. 4. *Region II*: stress profile for different cases. The solid thick line is for $t=1$ and $r=1$ (isotropic case), the thick dashed line is for $t=1$ and $r=2.125$, and the solid thin line is for $t=2$ and $r=1.5$.

the hyperbolic-elliptic boundary (see also Sec. IV B for further remarks). Inside region III, the fact that all roots are real excludes the possibility to require stresses to vanish for large z. This leads to a situation where there are more constants of integration than boundary conditions.

One may advance on the analytical form of response functions using physical arguments as follows. Let us first rewrite the equation for stresses (21), as follows:

$$(\partial_z^2-c_+^2\partial_x^2)(\partial_z^2-c_-^2\partial_x^2)\sigma_{ij}=0, \tag{44}$$

where

$$c_\pm^2=-r\pm\sqrt{r^2-t}, \tag{45}$$

leading to $c_\pm \geqslant 0$. The constants $\pm c_\pm$ are just the four real roots X_k mentioned above. Instead of solving the equation above, we consider special solutions σ_{ij}^+, σ_{ij}^- of the following partial differential equation:

$$(\partial_z^2-c_\pm^2\partial_x^2)\sigma_{ij}^\pm=0, \tag{46}$$

which automatically satisfy Eq. (44). Both equations can be solved for the boundary conditions (32) and (33), giving the solutions

$$\sigma_{zz}^\pm=\frac{F_0}{2}\left(\left[\cos\theta_0-\frac{\sin\theta_0}{c_\pm}\right]\delta(x+c_\pm z)+\left[\cos\theta_0+\frac{\sin\theta_0}{c_\pm}\right]\delta(x-c_\pm z)\right), \tag{47}$$

$$\sigma_{xz}^\pm=\frac{F_0}{2}\{-[c_\pm\cos\theta_0-\sin\theta_0]\delta(x+c_\pm z)+[c_\pm\cos\theta_0+\sin\theta_0]\delta(x-c_\pm z)\}, \tag{48}$$

$$\sigma_{xx}^\pm=\frac{F_0}{2}\{c_\pm[c_\pm\cos\theta_0-\sin\theta_0]\delta(x+c_\pm z)+c_\pm[c_\pm\cos\theta_0+\sin\theta_0]\delta(x-c_\pm z)\}. \tag{49}$$

Before constructing a general solution from $\sigma_{ij}^\pm$, let us remark that there are, in principle, additional solutions $\tilde{\sigma}_{ij}$ satisfying

$$(\partial_z^2-c_\pm^2\partial_x^2)\tilde{\sigma}_{ij}=\sigma_{ij}^\mp. \tag{50}$$

However, these solutions are not finite as they involve divergences arising from integrals such as $\int_{-\infty}^{\infty}dq\cos(qu)/q^2$. Therefore, we conclude that a general solution of Eq. (44) may be constructed as

$$\sigma_{ij}=a_+\sigma_{ij}^+ + a_-\sigma_{ij}^-. \tag{51}$$

It should satisfy the boundary conditions (32) and (33), which yield a relation

$$a_+ + a_-=1. \tag{52}$$

The coefficients a_+ and $a_-=1-a_+$ are relative weights which indicate how the applied load is shared between the two sets of force chains characterized by $c_\pm$. As there is no physical mechanism introduced *a priori* which prefers one set of force chains to the other, we are left with one free parameter, say a_+, for the response function σ_{ij}. The ambiguity on the value of a_+ could be resolved by considering e.g., a microscopic model that leads to Eq. (44).

In Fig. 5, the propagation of the applied force along the characteristics is shown. Note that the sign of σ_{zz} may change along a certain characteristic if $\cos\theta_0-(\sin\theta_0)/c_\pm<0$ [see Fig. 5(b)].

B. Anisotropy at an angle

We now, for completeness, generalize the results of the previous sections to the case where the direction of the anisotropy makes an arbitrary angle τ with the vertical. (The preceding section corresponds to $\tau=0$.) This situation may be relevant for systems that are initially sheared as in the experiments of Geng *et al.* [27], or prepared in a way which breaks the symmetry $x\leftrightarrow -x$. We restrict the discussion to regions I and II (the computation for region III can be carried out in a similar fashion).

The equivalent of the relation (7) involves now a matrix Λ_τ which is related to $\Lambda_\dagger$ of Eq. (13) by

$$\Lambda_\tau=\mathcal{Q}^{-1}\Lambda_\dagger\mathcal{Q}, \tag{53}$$

where $\mathcal{Q}$ is the rotation matrix

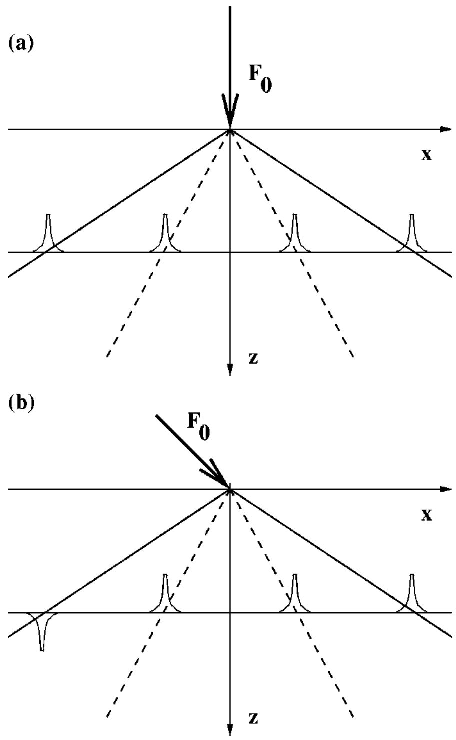

FIG. 5. *Region III*: the stress profile as a sum of four δ functions. The characteristics $x=\pm c_{\pm}z$ along which the applied load is propagated are shown. Parameters are $r=-1.0$, $t=0.75$ giving $c_+=1.5$ (solid lines) and $c_-=0.5$ (dashed lines). The δ functions are indicated by cartoons. (a) $\theta_0=0$, (b) $\theta_0=\pi/4$.

$$\mathcal{Q}=\begin{pmatrix} \cos^2\tau & \sin^2\tau & -2\sin\tau\cos\tau \\ \sin^2\tau & \cos^2\tau & +2\sin\tau\cos\tau \\ \sin\tau\cos\tau & -\sin\tau\cos\tau & \cos^2\tau-\sin^2\tau \end{pmatrix}. \tag{54}$$

The differential equation on the stress components that is deduced from the compatibility condition and stress-strain relations is now much more complicated, but the corresponding roots of the fourth-order polynomial that appear when looking at Fourier modes can still be calculated from the X_k solutions of Eq. (26). They read

$$Y_k=\frac{X_k-\tan\tau}{1+X_k\tan\tau}, \quad k=1,\ldots,4. \tag{55}$$

The same method as above (see also Appendix B) can then be applied to find the stress response functions for a localized overload at the top surface of the material. Note that the material properties are still determined by the X_k associated with $\Lambda_\dagger$. In particular, whether the response is elliptic or hyperbolic cannot depend on τ. In the following, regions I and II are defined with respect to X_k as above.

1. Region I

The X_k are of the form $\pm\beta\pm i\alpha$, see Eqs. (28) and (29). The corresponding Y_k can be constructed with the following quantities

$$A=\frac{\alpha(1+\tan^2\tau)}{(1+\beta\tan\tau)^2+(\alpha\tan\tau)^2}, \tag{56}$$

$$B=\frac{\beta(1-\tan^2\tau)+\tan\tau(\alpha^2+\beta^2-1)}{(1+\beta\tan\tau)^2+(\alpha\tan\tau)^2}, \tag{57}$$

$$A'=\frac{\alpha(1+\tan^2\tau)}{(1-\beta\tan\tau)^2+(\alpha\tan\tau)^2}, \tag{58}$$

$$B'=\frac{\beta(1-\tan^2\tau)-\tan\tau(\alpha^2+\beta^2-1)}{(1-\beta\tan\tau)^2+(\alpha\tan\tau)^2}. \tag{59}$$

The same boundary conditions (see Fig. 2) lead to

$$\begin{aligned}\sigma_{zz}=&\frac{F_0}{2\pi}\frac{2z^2}{[(x+Bz)^2+(Az)^2][(x-B'z)^2+(A'z)^2]}\\ &\times\{x\sin\theta_0(A+A')+z\cos\theta_0[AA'(A+A')+AB'^2\\ &+A'B^2]+[x\cos\theta_0+z\sin\theta_0](A'B-AB')\}.\end{aligned} \tag{60}$$

σ_{xz} and σ_{xx} are related to σ_{zz} by the usual factors of x/z and $(x/z)^2$, respectively.

Figures 6 and 7 show the pressure response profile as different parameters are varied. In Fig. 6 the applied force is kept vertical ($\theta_0=0$), and τ is varied from 0 to $\pi/4$. Interestingly, the initially double-peaked profile [Fig. 6(a)] is progressively deformed in such a way that the left peak gets more pronounced, until the remaining single peak moves to the right for $\tau=\pi/4$. This behavior might be counterintuitive for smaller τ, because a positive value of τ means that the main direction of the anisotropy is oriented to the right. However, it can be understood within the ball-and-spring model of Sec. IV, where the k_1 springs are horizontal. Rotating to the right the two stiff directions k_2 emerging from a ball downwards brings the left one closer to the vertical direction, which therefore gets a larger fraction of the overload. Continuing past $\tau=\pi/6$, however, the stiffer springs form lines that slope downward to the right. Since they continue to support most of the load, the single peak is shifted to the right. This behavior holds also for the single-peaked profiles of Fig. 6(b).

The second series of plots (Fig. 7) is for the case where the applied force is exactly in the direction of the anisotropy ($\theta_0=\tau$). The corresponding curves are qualitatively similar to those of Fig. 6. The direction of the force imposed at the top does not change the general shape (anisotropic double or single peak) except for the fact that a negative pressure zone evolves for large negative x.

The value of 0.6 for t used in the Figs. 6 and 7 is motivated by experimental findings [28]. The response function shown in Fig. 6(b) for $\tau=\pi/4$ is at least qualitatively consistent with the response functions measured in Ref. [27].

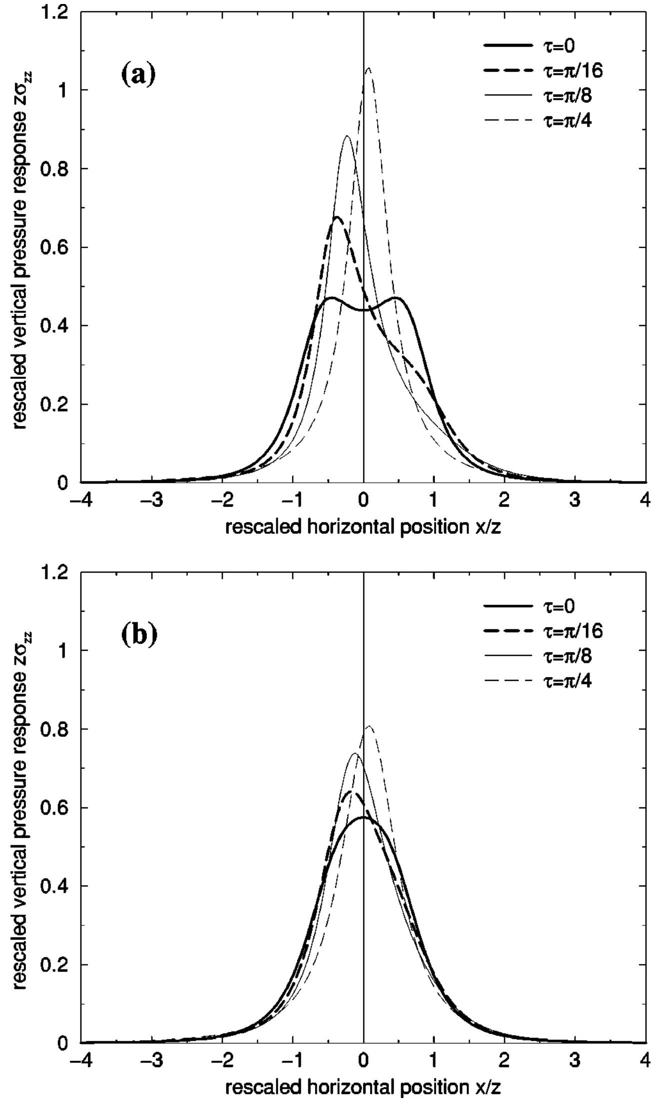

FIG. 6. *Region I*: response profiles for different values of the anisotropy angle τ, but with a fixed value for the orientation of the applied force: $\theta_0=0$. The graph (a) is for $t=0.6$ and $r=-0.2$, while (b) has been obtained for $t=0.6$ and $r=0.2$. Note that for the three smallest $\tau>0$ the response is stronger in the negative x region.

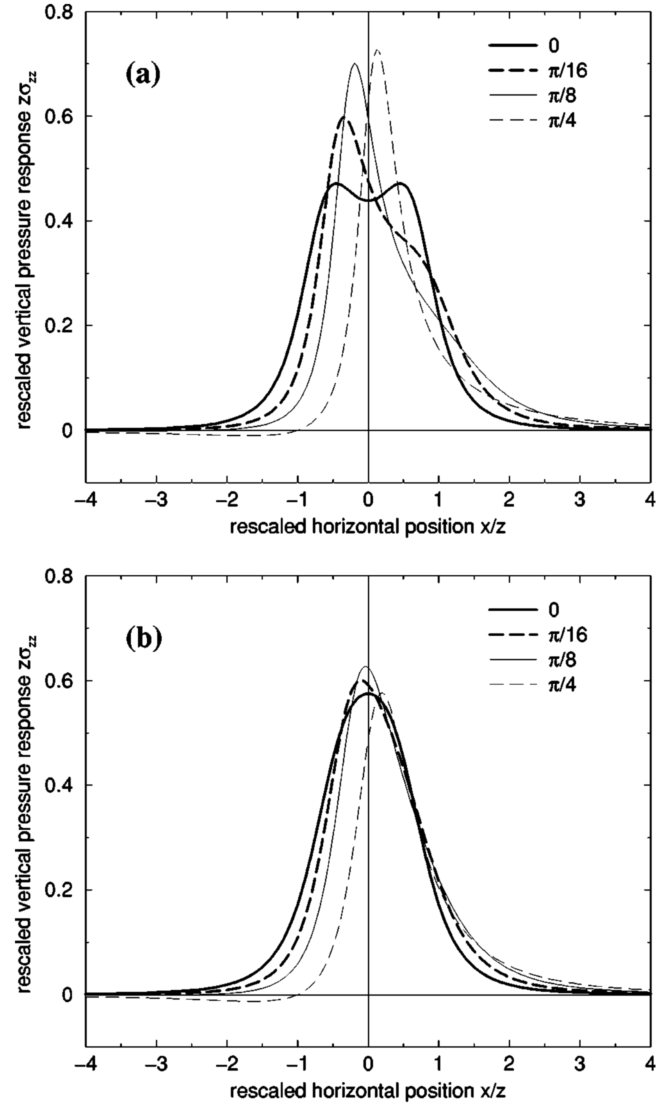

FIG. 7. Same graphs as in Fig. 6, but this time with $\theta_0=\tau$ as indicated in the legends.

2. Region II

In region II, where $X_1=-X_4=-i\alpha_1$ and $X_2=-X_3=-i\alpha_2$, the expressions of the corresponding Y_k involve the quantities

$$A_1=\frac{\alpha_1(1+\tan^2\tau)}{1+(\alpha_1\tan\tau)^2}, \tag{61}$$

$$B_1=\frac{\tan\tau(\alpha_1^2-1)}{1+(\alpha_1\tan\tau)^2}, \tag{62}$$

$$A_2=\frac{\alpha_2(1+\tan^2\tau)}{1+(\alpha_2\tan\tau)^2}, \tag{63}$$

$$B_2=\frac{\tan\tau(\alpha_2^2-1)}{1+(\alpha_2\tan\tau)^2}, \tag{64}$$

the pressure response having the form

$$\sigma_{zz}=\frac{F_0}{2\pi}\frac{2z^2}{[(x+B_1z)^2+(A_1z)^2][(x+B_2z)^2+(A_2z)^2]}\times\{x\sin\theta_0(A_1+A_2)+z\cos\theta_0[A_1A_2(A_1+A_2)+A_1B_2^2+A_2B_1^2]+[x\cos\theta_0+z\sin\theta_0](A_2B_1+A_1B_2)\}. \tag{65}$$

Again, the expressions of σ_{xz} and σ_{xx} are not shown, but can be deduced as usual from that of σ_{zz}.

Figures 8 and 9 show the response profile for different values of the parameters. Depending on these parameters, the response peak can be moved to the right or to the left with positive values of τ.

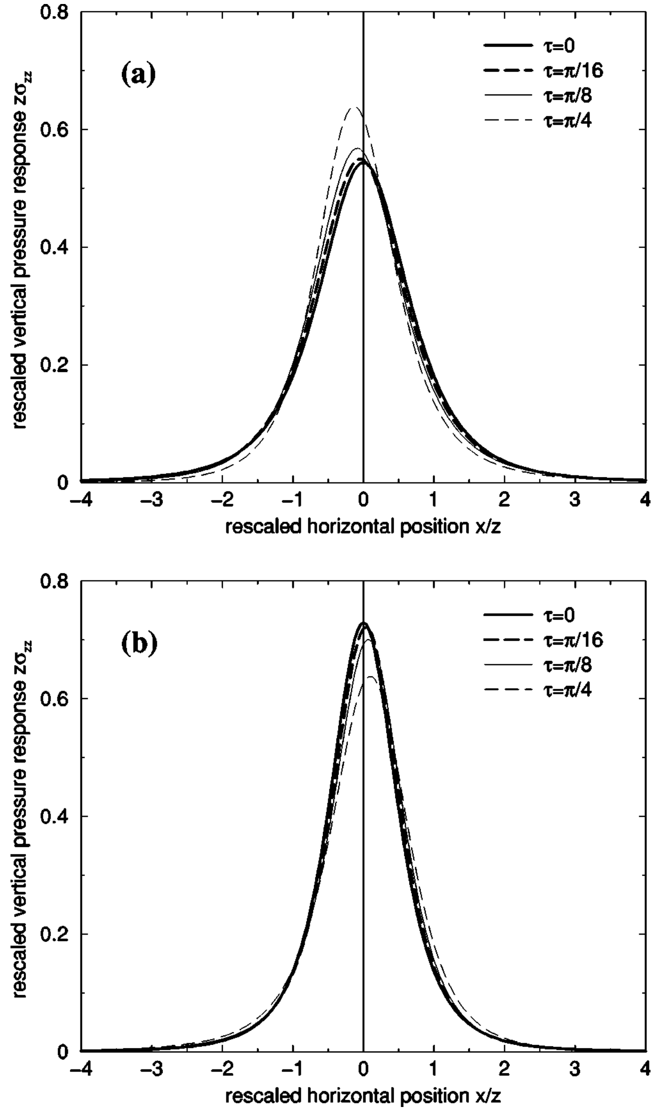

FIG. 8. *Region II*: response profiles for different values of the anisotropy angle τ, but with a fixed value for the orientation of the applied force: $\theta_0=0$. The graph (a) is now for $t=2$ and $r=1.5$, while (b) has been obtained for $t=0.6$ and $r=0.8$. This time, the response peak can be moved to the right or to the left with positive values of τ.

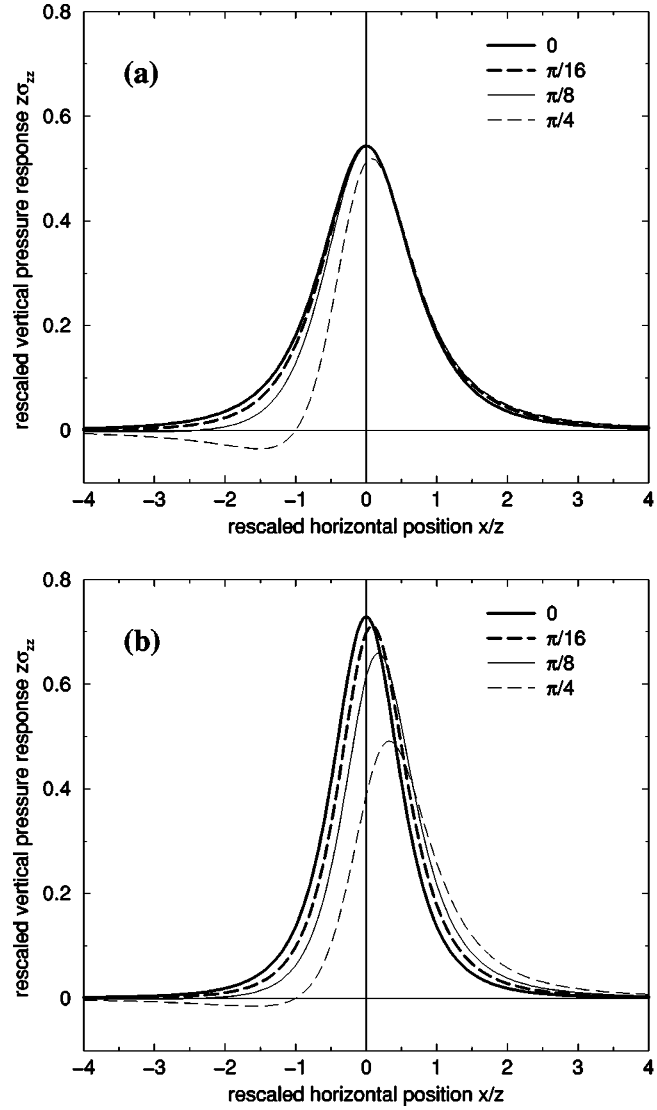

FIG. 9. Same graphs as in Fig. 8, but with $\theta_0=\tau$ as indicated in the legends.

Please note that the response function shown Fig. 8(b) for $\tau=\pi/4$ also agrees qualitatively with the experimental findings in Ref. [27]. A more detailed analysis of their results is certainly worthwhile, also in order to possibly decide whether region I or II behavior applies for a sheared two-dimensional layer where the angle of the preferred orientation of force chains coincides with $\tau=\pi/4$.

IV. TRIANGULAR SPRING NETWORKS AND ANISOTROPIC ELASTICITY

A. Triangular spring networks

To illustrate the previous calculations, it may be useful to construct a ball-and-spring model with a tunable parameter that allows us to obtain different relative values of a, b, c, and d above. Here, we consider a triangular lattice of balls with springs connecting all nearest-neighbor pairs. The lattice may be oriented in either of the two ways as shown in Fig. 10, and the springs have stiffnesses k_1 or k_2 as shown for the two cases. All springs lying along a given direction have the same stiffness. We take the equilibrium lengths of all springs to be unity.

In either orientation, the system has reflection symmetry under $x\rightarrow -x$ and $z\rightarrow -z$, but not under rotations; it is described by an anisotropic stress-strain relation involving $\Lambda_{\dagger}$.

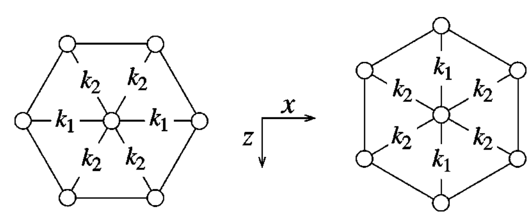

FIG. 10. Network of springs of stiffness k_1 and k_2.

We determine the elastic coefficients by writing down the energy directly for a homogeneous deformation. Note that the balls form a Bravais lattice, and hence that their displacements for a given average strain u_{ij} are simply given by $u_{ij}r_j$, where $\mathbf{r}$ is the equilibrium position of the ball. The energy density can easily be obtained by summing the energies of the three springs linking the ball at (0,0) to its neighbors along different lattice directions and dividing by the area of the unit cell, $A=\sqrt{3}/2$.

1. Horizontal orientation of the k_1 springs

For the case, where the k_1 spring is horizontal, we find for the energy density,

$$F=\frac{1}{16A}[(8k_1+k_2)u_{xx}^2+9k_2u_{zz}^2+6k_2u_{xx}u_{zz}+3k_2(u_{xz}+u_{zx})^2], \tag{66}$$

which corresponds to a matrix $\Lambda_\dagger$ with the following coefficients:

$$a=\frac{8k_1+k_2}{8A}, \tag{67}$$

$$b=\frac{9k_2}{8A}, \tag{68}$$

$$c=\frac{3k_2}{8A}, \tag{69}$$

$$d=\frac{6k_2}{8A}. \tag{70}$$

Without loss of generality, we rescale all stiffnesses by a factor $8A/k_2$ and let k_1/k_2 be denoted k. The coefficients r and t of Eq. (26) are then given by

$$t=\frac{1+8k}{9}, \tag{71}$$

$$r=\frac{4k-1}{3}, \tag{72}$$

which gives $r^2-t=\frac{16}{9}k(k-1)$. We may eliminate k from these two equations to obtain a trajectory in (r,t) space:

$$t=\frac{2r+1}{3}, \tag{73}$$

shown as the plain line in Fig. 1.

Thus, $k<1$ (weak horizontal springs) corresponds to region I above with [see Eq. (28)]

$$\alpha^2=\frac{1}{6}(4k-1+\sqrt{8k+1}), \tag{74}$$

$$\beta^2=\frac{1}{6}(1-4k+\sqrt{8k+1}). \tag{75}$$

As mentioned above, the condition for a double-peaked σ_{zz} profile is $r<0$. Hence, the single-peaked shape of $\sigma_{zz}(x)$ becomes double peaked when $k<1/4$, i.e., when the horizontal springs are substantially softer than the others.

For $k>1$, on the other hand, we are in region II with [see Eq. (30)]

$$\alpha_1^2=\frac{1}{3}[4k-1+4\sqrt{k(k-1)}], \tag{76}$$

$$\alpha_2^2=\frac{1}{3}[4k-1-4\sqrt{k(k-1)}]. \tag{77}$$

The σ_{zz} profile is always a single peaked when the horizontal springs are stiffer than the others.

2. Vertical orientation of the k_1 springs

For the case where the k_1 spring is vertical, we get a matrix $\Lambda_\dagger$ where the coefficients a and b have been swapped from the horizontal case, i.e., with the following coefficients:

$$a=\frac{9k_2}{8A}, \tag{78}$$

$$b=\frac{8k_1+k_2}{8A}, \tag{79}$$

$$c=\frac{3k_2}{8A}, \tag{80}$$

$$d=\frac{6k_2}{8A}. \tag{81}$$

Again, we rescale the stiffnesses and let $k=k_1/k_2$, this time finding

$$t=\frac{9}{1+8k}, \tag{82}$$

$$r=\frac{3(4k-1)}{1+8k}, \tag{83}$$

which gives $r^2-t=144\,k(k-1)/(1+8k)^2$. As before, k may be eliminated to obtain the trajectory in (r,t) space:

$$t=-2r+3, \tag{84}$$

now corresponding to the dotted line in Fig. 1.

For $k<1$, we are in region I with

$$\alpha^2=\frac{9k}{1+8k}, \tag{85}$$

$$\beta^2=\frac{3(1-k)}{1+8k}. \tag{86}$$

Again, the single-peaked shape of the σ_{zz} profile becomes double peaked when $k<1/4$.

For $k>1$, we have $r^2-t>0$ and we are in region II, with

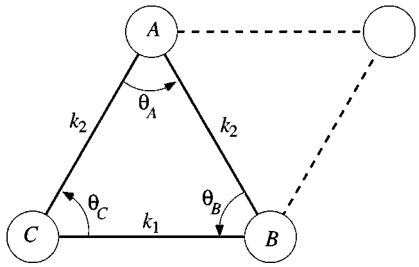

FIG. 11. Variables associated with three-body bond-bending interaction.

$$\alpha_1^2 = \frac{3}{1+8k}[4k-1+4\sqrt{k(k-1)}], \tag{87}$$

$$\alpha_2^2 = \frac{3}{1+8k}[4k-1-4\sqrt{k(k-1)}]. \tag{88}$$

3. Three-body (bond-bending) interactions

For the spring networks discussed above, the Poisson ratios are not both adjustable simultaneously. For the horizontal orientation of k_1 springs, $\nu_x = c/a$ is always 1/3, while for the vertical orientation $\nu_z = c/b$ is always 1/3. In order to have a ball-and-spring model on a Bravais lattice in which all elastic parameters can be varied independently, it is necessary to introduce three-body interactions. A straightforward way of doing this is to assume an energy cost for bond angles that differ from 60°.

For simplicity, we present an analysis only for the case where the triangular lattice is oriented so that the k_1 springs are horizontal. Consider the triangle of balls and springs shown in Fig. 11. We define θ_Y as $\angle XYZ$, measured in the strained configuration. For the case of uniaxial symmetry, the energy of the triangle is determined by two bond-bending stiffnesses κ_1 and κ_2. For case I, we define

$$E_{bb} = (1/2)\left[\kappa_1\left(\theta_A - \frac{\pi}{3}\right)^2 + \kappa_2\left(\theta_B - \frac{\pi}{3}\right)^2 + \kappa_2\left(\theta_C - \frac{\pi}{3}\right)^2\right], \tag{89}$$

with κ_1 assigned to the angle opposite the horizontal edge. As for Eq. (66), we take the equilibrium lengths of the springs to be unity.

Writing expressions for the angles in terms of displacements of the balls from their equilibrium positions and summing over all triangles, including the upside-down ones (shown dashed in Fig. 11) on a homogeneously strained lattice, we find a contribution to the total energy density of

$$F_{bb} = \frac{3}{8A}[(2\kappa_1+\kappa_2)(u_{xx}^2+u_{zz}^2) - 2(2\kappa_1+\kappa_2)u_{xx}u_{zz} + 12\kappa_2 u_{xz}^2]. \tag{90}$$

Adding this contribution to Eq. (66) gives a total energy density corresponding to a matrix $\Lambda_\dagger$ with coefficients

$$a = \frac{8k_1+k_2+6\kappa}{8A}, \tag{91}$$

$$b = \frac{9k_2+6\kappa}{8A}, \tag{92}$$

$$c = \frac{3k_2-6\kappa}{8A}, \tag{93}$$

$$d = \frac{6(k_2+6\kappa_2)}{8A}, \tag{94}$$

where $\kappa \equiv 2\kappa_1 + \kappa_2$. In terms of bulk and shear moduli and Poisson ratios, we obtain

$$E_z = \frac{9k_1k_2+6(k_1+2k_2)\kappa}{(8k_1+k_2+6\kappa)A}, \tag{95}$$

$$E_x = \frac{3k_1k_2+2(k_1+2k_2)\kappa}{(3k_2+2\kappa)A}, \tag{96}$$

$$G = \frac{6(k_2+6\kappa_2)}{8A}, \tag{97}$$

$$\nu_z = \frac{3k_2-6\kappa}{8k_1+k_2+6\kappa}, \tag{98}$$

$$\nu_x = \frac{k_2-2\kappa}{3k_2+2\kappa}. \tag{99}$$

Note that $E_x\nu_z = E_z\nu_x$, as expected. Note also that it is not necessary for k_1, k_2, κ_1, and κ_2 to all be positive. Stability [cf. Eq. (17)] requires only

$$8k_1+k_2+6\kappa > 0, \tag{100}$$

$$3k_2+2\kappa > 0, \tag{101}$$

$$3k_1k_2+2\kappa(k_1+2k_2) > 0, \tag{102}$$

$$k_2+6\kappa_2 > 0. \tag{103}$$

From Eq. (22), we find

$$t = \frac{8k_1+k_2+6\kappa}{3(3k_2+2\kappa)}, \tag{104}$$

$$r = 1 + \left(\frac{4}{3}\right)\frac{3k_1k_2+2\kappa(k_1+2k_2)}{(3k_2+2\kappa)(k_2+6\kappa_2)} - \frac{4k_2}{3k_2+2\kappa}. \tag{105}$$

By choosing k_1, k_2, and κ, we can obtain any positive value for t. From Eqs. (100)–(103), we see that the second term in the expression for r is positive. For fixed t, we can make r arbitrarily large by choosing κ_2 close to $-k_2/6$. The smallest (or largest negative) value of r is obtained by choosing

$3k_1k_2+2\kappa(k_1+2k_2)=0$ (and adjusting k_1, say, to keep t fixed). This leads to $r^2-t=0$ and $r<0$, demonstrating that the triangular lattice can lie anywhere in region I or II.

B. Remarks

We have seen that classical anisotropic elastic materials can have double-peaked response functions and that such cases can be obtained with simple ball-and-spring models. These calculations explain, for example, the numerical results of Goldenberg and Goldhirsch [18], without invoking any special considerations on small system sizes.

It is important to note that the response functions for the triangular spring networks always lie in the elliptic regime: the peaks broaden linearly with depth. Thus, the observation of a double-peak structure is *not* necessarily an indication of propagative (hyperbolic) response in an elastic material. However, when the k_1 springs are oriented horizontally, and in the limit where their stiffness tends to zero, the response becomes hyperbolic. In this case, one generically expects peaks to broaden diffusively, i.e., like $\sqrt{Dz}$ [6,25]. Note that in the limit where $k_1\to 0$, there appears a floppy (zero energy) extended deformation mode which, as emphasized by Tkachenko and Witten [10], naturally leads to a stress-only closure equation and hyperbolicity. In the phase diagram, Fig. 1, this limit corresponds to the point where the straight solid line touches the boundary curve $t=r^2$. Note that within this line of thought, one should also expect hyperbolic response in elastic percolation networks at the rigidity threshold. In fact, in the limit $k_1\to 0$ the triangular network becomes a rhombic network which is known to become isostatic for a finite system: a single boundary suffices (say a bottom surface in the slab geometry) in order to suppress the zero mode, and the system becomes rigid [9].

V. ANISOTROPIC DIRECTED-FORCE CHAIN NETWORKS

A. Biased scattering

In Ref. [13], a Boltzmann equation for the chain-splitting model was derived for a granular medium which is strongly disordered. In the present work, we suppose that the scattering of force chains by defects is biased by a preferred orientation of the material, modeled in terms of a global director $\mathbf{N}$. We intend to describe systems possessing a uniaxial symmetry, which have undergone compaction or shearing or which have been constructed by sequential avalanching due to grains poured from a horizontally moving orifice.

The fundamental quantity is the distribution function $P(f,\mathbf{n},\mathbf{r})$, where

$$P(f,\mathbf{n},\mathbf{r})\,df\,d\mathbf{n}\,d^Dr \tag{106}$$

gives the number of force chains with intensity between f and $f+df$, inside the (solid) angle $d\mathbf{n}$ around the direction $\mathbf{n}$, in a small volume element d^Dr centered at $\mathbf{r}$. Integration of $P(f,\mathbf{n},\mathbf{r})$ with respect to f and $\mathbf{n}$ will yield the density of force chains at the point $\mathbf{r}$. [30] The distribution function is defined with respect to an ensemble of different realizations of force chains for an assumed uniform spatial distribution of point defects (of density ρ_d), with same boundary conditions. In the spirit of previous models [7,26] that give hyperbolic equations for the stresses, a mechanism of propagation is implemented, but now on the local level of force chains. In the analytical model presented here, a pairwise merger of force chain to a single one will be neglected. The limitation of this approximation will be discussed below. Then the distribution function $P(f,\mathbf{n},\mathbf{r})$ obeys the following linear equation:

$$P(f_1,\mathbf{n}_1,\mathbf{r}+\mathbf{n}_1dr)=\left(1-\frac{dr}{\lambda}\right)P(f_1,\mathbf{n}_1,\mathbf{r})+2\frac{dr}{\lambda}\int df'\int df_2\int d\mathbf{n}'\int d\mathbf{n}_2P(f',\mathbf{n}',\mathbf{r})\Psi(\mathbf{n}'\to\mathbf{n}_1,\mathbf{n}_2|\mathbf{N})$$
$$\times\,\delta(f_1\cos\theta_1+f_2\cos\theta_2-f')\,\delta(f_1\sin\theta_1+f_2\sin\theta_2)|\sin(\theta_1-\theta_2)|, \tag{107}$$

where λ is the mean free path of force chains, and is of the order of $1/(\rho_d l^{D-1})$ in D dimensions. The length l represents the average size of a grain. The equation means the following: a force chain at some point $\mathbf{r}+\mathbf{n}_1dr$ is either due to an unscattered force chain, which occurs with the probability that no scattering occurs times the probability that the same force chain existed at point $\mathbf{r}$ (given by the first term on the right-hand side (rhs) of the equation), or to a scattered force chain. The latter occurs with the probability given by the second term on the rhs of the equation: it is the sum with respect to all intensities and directions of the incoming (labeled by a prime) and the second outgoing force chains of the product of the probability for the incoming force chain to arrive at $\mathbf{r}$ times the probability of scattering $(dr/\lambda)\Psi(\mathbf{n}'\to\mathbf{n}_1,\mathbf{n}_2|\mathbf{N})$. The δ functions impose conservation of forces, the factor 2 accounts for the number of outgoing force chains, and the factor $|\sin(\theta_1-\theta_2)|$ is convenient to write explicitly rather than include in Ψ. The dependence of the scattering probability on $\mathbf{N}$ requires to consider the outgoing force chains separately. In the absence of $\mathbf{N}$ the outgoing force chains may be treated symmetrically, and one recovers the linear model for an isotropic medium [13].

The analytical model presented for biased force chain scattering does not take into account fusion of force chains, which leads, in general, to a nonlinear Boltzmann equation. For an isotropic medium the consequences of fusion have been discussed for a model where force chains are restricted to lie on exactly six directions [14]. In this discrete model the validity of the linear approximation was explicitly shown to be restricted to shallow systems (depths smaller than a few times λ) and small forces. However, preliminary results on a discrete model with eight directions suggest that the linear theory might have a wider scope of application than expected from the study on the six-leg model. More precisely, a proper analysis of the linear perturbation analysis around the full nonlinear solution of the Boltzmann equation might share, in some regimes, many properties of the linear solution presented here. In any case, one can see the present analysis as a shallow layer approximation where the fusion of chains can indeed be neglected.

Instead of solving Eq. (107), we first introduce the scalar local average force density $F(\mathbf{n},\mathbf{r})$, i.e., the local scalar force field per unit volume, defined as

$$F(\mathbf{n},\mathbf{r})=\int_0^\infty df\, fP(f,\mathbf{n},\mathbf{r}). \tag{108}$$

Then, multiplying Eq. (107) by f, we obtain the following equation for $F(\mathbf{n}_1,\mathbf{r})$:

$$\lambda \mathbf{n}_1\cdot\boldsymbol{\nabla}_r F(\mathbf{n}_1,\mathbf{r}) = -F(\mathbf{n}_1,\mathbf{r})+2\int d\mathbf{n}'\int d\mathbf{n}_2 F(\mathbf{n}',\mathbf{r})\Psi(\mathbf{n}'\to\mathbf{n}_1,\mathbf{n}_2|\mathbf{N}) \times\frac{1}{\cos\theta_1-(\sin\theta_1/\sin\theta_2)\cos\theta_2}. \tag{109}$$

This equation is identical in form to the Schwarzschild-Milne equation for radiative transfer [31], though, unlike the situation in radiative transfer problems, the albedo is larger than unity. Let us note that the possibility to rewrite the Boltzmann-type equation (107) in terms of the force density $F(\mathbf{n},\mathbf{r})$ is only possible for the linear model.

From now on, we take all lengths in units of l which amounts to formally setting $l=1$. Now, we introduce physically relevant angular averages

$$p(\mathbf{r})=\int d\mathbf{n}F(\mathbf{n},\mathbf{r}), \tag{110}$$

$$J_i(\mathbf{r})=\int d\mathbf{n}n_iF(\mathbf{n},\mathbf{r}), \tag{111}$$

$$\sigma_{ij}(\mathbf{r})=D\int d\mathbf{n}n_in_jF(\mathbf{n},\mathbf{r}), \tag{112}$$

where $\int d\Omega$ is a normalized integral over the unit sphere. The field p is the isostatic pressure, while $\mathbf{J}$ may be interpreted as the local directed average force chain intensity per unit surface. Now, given a local snapshot of a force chain network, one can usually not tell the direction of each chain. Moreover, the average force vanishes everywhere in the system as a consequence of Newton's third law. The directions of chains are actually determined by the boundary conditions, say on the top and bottom of a granular layer, which thereby determine the field $\mathbf{J}$ in the bulk. It is the propagation of force chains starting from the boundaries of the system modeled by Eq. (107) which leads to the orientation of the force chain network. Finally, the tensor σ is the stress tensor.

B. Stress equilibrium at large length scales

We now proceed to obtain the equations governing the physically relevant fields introduced above, by calculating the zeroth, first, and second moment with respect to n_i of Eq. (109). The equations read as

$$\lambda\boldsymbol{\nabla}\cdot\mathbf{J}=(c_1-1)p+c_2\sigma_{NN}, \tag{113}$$

$$\partial_j\sigma_{ij}=0, \tag{114}$$

$$\frac{\lambda}{(D+2)}(\delta_{ij}\boldsymbol{\nabla}\cdot\mathbf{J}+\partial_iJ_j+\partial_jJ_i) =B_0\sigma_{ij}+\delta_{ij}(B_1\lambda\boldsymbol{\nabla}\cdot\mathbf{J}+B_2\sigma_{NN})+\mathbf{N}_i\mathbf{N}_j(B_3\lambda\boldsymbol{\nabla}\cdot\mathbf{J} +B_4\sigma_{NN})+B_5(N_i\sigma_{jk}N_k+N_j\sigma_{ik}N_k), \tag{115}$$

where $\sigma_{NN}=\mathbf{N}\cdot\sigma\cdot\mathbf{N}$. The second equation (114) is readily obtained upon averaging, while the first and third, equations (113) and (115), are obtained using an Chapman-Enskog-type expansion of the local average force density $F(\mathbf{n},\mathbf{r})$ in terms of the fields p, $\mathbf{J}$, and σ already given in Ref. [13]:

$$F(\mathbf{n},\mathbf{r})=p(\mathbf{r})+D\mathbf{n}\cdot\mathbf{J}(\mathbf{r})+\frac{D+2}{2}\mathbf{n}\cdot\hat{\sigma}(\mathbf{r})\cdot\mathbf{n}+\cdots. \tag{116}$$

Let us remark that Eq. (114) gives mechanical equilibrium as expected and is independent on the specific form of $\Psi(\mathbf{n}'\to\mathbf{n}_1,\mathbf{n}_2|\mathbf{N})$. The validity of the Chapman-Enskog expansion is based on the assumption that on large enough length scale an isotropic state is reached. For the case of biased scattering of force chains considered here, this implies that the bias intensity must not be too strong. Then the statistical weight of the set of force chains propagating through the entire system without changing their direction will not be important. The limiting case of strong bias requires a different approach than the one presented here.

The constants c_μ and B_μ appearing in Eqs. (113) and (115), respectively, are angular integrals involving the microscopic model for the scattering process, i.e., a specification of $\Psi(\mathbf{n}'\to\mathbf{n}_1,\mathbf{n}_2|\mathbf{N})$. A specific model will be considered in Sec. V D. If one neglects the dependence on $\mathbf{N}$ in the equations above, one recovers the simpler equations for force chain splitting in an isotropic granular medium [13].

C. A linear pseudoelastic theory

As in the isotropic case, one would like to see if Eq. (115) can be cast into a form where the stress tensor σ_{ij} is a linear function of a pseudostrain tensor

$$u_{ij}\propto\frac{1}{2}(\partial_iJ_j+\partial_jJ_i), \tag{117}$$

giving rise to the relation

$$\sigma_{ij}=\lambda_{ijkl}u_{kl}, \tag{118}$$

where λ_{ijkl} is the anisotropic pseudoelastic modulus tensor. Similarly to conventional elasticity theory as mentioned in

Sec. II, we will see that the tensor λ_{ijkl} satisfies the symmetries given in Eq. (2). The symmetric form of u_{ij} stems from the symmetries appearing in the derivation of the large scale equations when carrying out angular averages, in particular, $\int d\mathbf{n} n_i n_j n_k n_l$. In Eq. (115), the gradients of the field J_i appear only in combinations such as $\boldsymbol{\nabla}\cdot\mathbf{J}$ and $\partial_i J_j + \partial_j J_i$. Please note, however, that unlike in classical anisotropic linear elasticity theory, in the present case,

$$\lambda_{ijkl} \neq \lambda_{klij}, \tag{119}$$

except for certain cases imposed by the details of the scattering process. The absence of the symmetry present in the classical theory is possible because there is no underlying free energy functional.

The relation between the stress tensor and the pseudoelastic strain tensor can be derived using the second moment Eq. (115). The latter can be rewritten in the following form:

$$J_{ij} = B_{ijkl}\sigma_{kl}, \tag{120}$$

where

$$J_{ij} = \lambda \boldsymbol{\nabla}\cdot\mathbf{J}\left[\delta_{ij}\left(\frac{1}{D+2} - B_1\right) - B_3 N_i N_j\right] + \frac{\lambda}{D+2}(\partial_i J_j + \partial_j J_i) \tag{121}$$

and

$$B_{ijkl} = \frac{B_0}{2}(\delta_{ik}\delta_{jl} + \delta_{il}\delta_{jk}) + B_2\delta_{ij}N_k N_l + \frac{B_5}{2}(\delta_{jl}N_i N_k + \delta_{jk}N_i N_l + \delta_{ik}N_j N_l + \delta_{il}N_j N_k) + B_4 N_i N_j N_k N_l. \tag{122}$$

The relation between J_{ij} and σ_{kl} can be inverted to give

$$\sigma_{ij} = \frac{1}{2}A_{ijkl}J_{kl}, \tag{123}$$

where A_{ijkl} has the same form as B_{ijkl} with the constants B_μ being replaced by constants A_μ which are obtained from the relation

$$A_{ijkl}B_{klmn} = I_{ijmn} = \delta_{im}\delta_{jn} + \delta_{in}\delta_{jm}. \tag{124}$$

In particular, one obtains the following relations for the constants A_μ:

$$A_0 = \frac{2}{B_0}, \tag{125}$$

$$A_2 = -\frac{2B_2}{B_0(B_0+B_2+B_4+2B_5)}, \tag{126}$$

$$A_4 = \frac{\left(-2B_4 + \frac{4B_5}{(B_0+B_5)}(B_2+B_4+B_5)\right)}{B_0(B_0+B_2+B_4+2B_5)}, \tag{127}$$

$$A_5 = -\frac{2B_5}{B_0(B_0+B_5)}. \tag{128}$$

Now, one can finally determine the pseudoelastic modulus tensor in terms of the tensor A_{ijkl},

$$\lambda_{ijkl} = \frac{\lambda}{D+2}\left(A_{ijkl} + \frac{1}{2}A_{ijmm}\delta_{kl}\right) - \frac{\lambda}{2}(B_1 A_{ijmm} + B_3 A_{ijmn}N_m N_n)\delta_{kl}. \tag{129}$$

Thus, the pseudoelastic modulus tensor λ_{ijkl} becomes—via the tensor A_{ijkl} and the constants A_μ—a function of the constants B_μ which depend on the specific scattering model used.

In the following section, a special case will be studied which allows us to derive a simple, but nontrivial equation for the stresses which supplemented by the mechanical equilibrium condition (114) opens a way to determine the stress tensor, or, put differently, the response function.

D. A microscopic model for force chain splitting in the presence of a bias

As mentioned in the preceeding section, the entries of the pseudoelastic modulus tensor depend on the specific model for anisotropic scattering which is specified in terms of the scattering cross section conditional on the global director $\mathbf{N}$, $\Psi(\mathbf{n}'\to\mathbf{n}_1,\mathbf{n}_2|\mathbf{N})$. We have considered a specific model for force chain splitting. It tunes the strength of the bias for scattering parallel to $\mathbf{N}$, using a weight for each outgoing chain proportional to powers of a cosine factor quantifying the degree of collinearity with the global director $\mathbf{N}$ (see Fig. 12).

For each force chain arriving at a defect in the direction $\mathbf{n}'$ two outgoing force chains are chosen in the directions $\mathbf{n}_1$ and $\mathbf{n}_2$ as follows: the angle of one chain, say number 1, with respect to the incoming force chain is chosen with weight $\propto(\mathbf{n}_1\cdot\mathbf{N})^{2p}$, for a positive integer p, in the interval $[0,\theta_{max}]$ (or $[-\theta_{max},0]$), while the other outgoing chain, say 2, is chosen uniformly in the interval $[-\theta_{max},\theta_1]$ (or $[-\theta_1,\theta_{max}]$, respectively). The reason for choosing the direction of the second chain like this is that the first (biased) chain should carry most of the intensity of the incoming force. Increasing p leads to scattering which is more and more biased in the the direction $\mathbf{N}$. The form of the scattering cross section is therefore chosen as

$$\Psi(\mathbf{n}'\to\mathbf{n}_1,\mathbf{n}_2|\mathbf{N}) = C_p[\psi(\theta_2|\theta_1)(\mathbf{n}_1\cdot\mathbf{N})^{2p} + \psi(\theta_1|\theta_2)\times(\mathbf{n}_2\cdot\mathbf{N})^{2p}]. \tag{130}$$

The functions $\psi(\theta_i|\theta_j)$ are the respective (uniform) probabilities for θ_i given θ_j described above. The constant C_p is a normalization factor which depends on the angle between $\mathbf{n}'$ and $\mathbf{N}$ and which is determined from

$$\int d\mathbf{n}_1 \int d\mathbf{n}_2 \Psi(\mathbf{n}'\to\mathbf{n}_1,\mathbf{n}_2|\mathbf{N}) = 1, \tag{131}$$

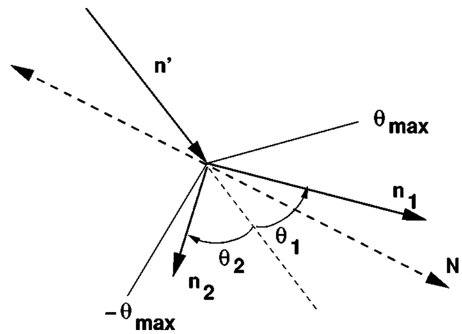

FIG. 12. The microscopic scattering model. The length of the arrows are different to illustrate the amount of force transmitted along the directions.

and its explicit form is given in Appendix A 4.

The simplest choice for the global director is $\mathbf{N}=\hat{z}$, i.e., if force chains are scattered preferably downward. We might think of a granular layer that has undergone compaction by a vertical load. In this case, the matrix $\Lambda_{\dagger}$ relating the stress and pseudostrain tensor has the block-diagonal form as given in Eq. (13). Any other orientation of $\mathbf{N}$ can be related to the vertical one by an appropriate rotation [see Sec. III B, Eq. (53)].

The numerical values of the parameters r and t that determine the shape of the response function (see Fig. 1) depend in the case of the anisotropic linear directed-force chain network model on the constants B_{μ} introduced in the preceding section. The latter are calculated from the above microscopic scattering model (see Appendix A) and are listed in Tables I–IV of Appendix A for different choices of the maximum angle θ_{max} of the scattering cone and different bias intensities p.

Interestingly, the roots we find for this scattering model all lie in the (elliptic) regions I and II introduced in Fig. 1. Hence, it is possible to find an anisotropic scattering rule that leads to a two-peak structure of the response function, but in no cases the values of r and t have been found to lie in the hyperbolic region. Whether this is a limitation of the linear treatment of the DFCN, as suggested by the analysis of the six-fold model [14], is at present not settled. Work in this direction is underway [32].

We finish this section with the following remark. If one identifies the elastic constants of classical anisotropic elasticity theory and their geometrical generalizations obtained for the linear anisotropic DFCN, as we have always done implicitly here, the possible range of values which occur for typical granular materials can be discussed. Experiments indicate that in samples of sand which are filled from above and where the major principal axis of a stress tensor is in the vertical direction, $t=E_x/E_z$ attains values in the range $0.4<t<1$ (see Ref. [33]). For the maximum scattering angles plotted in Fig. 1, the values of t determined from the specific microscopic model for biased force chain scattering used here appear to satisfy the experimental range. Further information on the construction history of the sand samples, which affects, e.g., the distribution of packing defects or the strength of the scattering bias, is needed to fully judge the quality of the anisotropic DFCN model presented here.

VI. CONCLUSION

The main objective of this paper was to work out in details the response function to a localized overload in the case of linear anisotropic elastic, or pseudoelastic materials in two dimensions.

After working out the details of two specific microscopic models, a triangular network of springs and an anisotropic directed force network, we have shown that the resulting large scale equations can lead to a large variety of response profiles, summarized in the phase diagram shown in Fig. 1 spanned by a two-parameter combination of entries of the (pseudo-)elastic modulus tensor. The one-peak structure of conventional (elliptic) isotropic elasticity can split into two peaks for sufficiently anisotropic materials. This situation occurs as soon as the shear modulus G is greater than the ratio $E_x/\nu_x=E_z/\nu_z$ of the Young modulus and the Poisson ratio (either in vertical or horizontal direction). This corresponds to an anisotropic material for which vertical stresses are easily transformed into horizontal strain (large Poisson ratios) and vice versa but which strongly resists shear stresses. However, contrarily to the prediction of stress-only hyperbolic models, these two peaks generically spread proportionally to the height of the layer, and not as the square root of the height for an hyperbolic medium. For the triangular network of springs, there is a special point, where the lattice loses its rigidity and a soft mode appears, where the system becomes exactly hyperbolic. It would be interesting to exhibit other situations where these extended soft modes discussed in Ref. [10] naturally appear; a possible candidate is a percolating network of springs at rigidity percolation.

For the anisotropic rules of force chain scattering that we have chosen, on the other hand, the directed-force network was always found to be in the elliptic regime. This might, however, be an artifact of the linear approximation that we have used and where mergers of force chains are ignored. Preliminary results suggest that for the full nonlinear problem, a genuine elliptic to hyperbolic phase transition might take place when the degree of anisotropy is increased, but more work (underway) is needed to confirm this potentially interesting result.

Recent experiments [27] have not been able so far to distinguish between a noisy hyperbolic response (where the width of peaks scales as the square root of the height) or anisotropic (pseudo)elastic response functions. For sheared system where force chains are preferably oriented at 45° with respect to the vertical, response functions show a horizontal shift (in the lateral direction with respect to the point of applied force) of the maximum, consistent with the preferred orientation of force chains. We found qualitative agreement with our findings. More detailed experiments appear to be necessary to decide on the parameters r,t, i.e., the possible locations in the phase diagram, Fig. 1, or put differently on the elastic constants, corresponding to a particular form of the response function, if the present (pseudo)elastic analysis applies.

It would be interesting to extend the present results to three-dimensional situations in order to fit the results of experiments on deep sand layers, where a single-peak response function was measured [16], and, most importantly, to test the consistency of the effective elastic moduli obtained from this fit in other geometries (like the sandpile or the silo). It would also be very interesting to find a way to prepare a disordered granular medium in a sufficiently anisotropic state such as to observe a two-peak response functions.

ACKNOWLEDGMENTS

We wish to thank B. Behringer, M. Cates, E. Clément, C. Gay, I. Goldhirsch, E. Kolb, D. Levine, J. M. Luck, C. Moukarzel, G. Ovarlez, G. Reydellet, D. Schaeffer, R. da Silveira, and J. P. Wittmer for very useful discussions. We thank C. Gay for pointing out the papers by Green *et al.* to us. M.O. is very grateful to the Service de Physique de l'État Condensé at CEA, Saclay, where most of this work was performed, for hospitality and a stimulating atmosphere, and acknowledges financial support from DFG Grant No. OT 201/1-1 J.E.S.S. acknowledges support from NSF through Grant No. DMR-01-37119.

APPENDIX A: SOME INTEGRALS FOR BIASED LINEAR DFCN

1. Zeroth moment

First, we propose to calculate the coefficients c_1 and c_2. Using the expansion (116) the integral with respect to $\mathbf{n}_1$ of the equation for the force density, one finds

$$\begin{aligned}\lambda \boldsymbol{\nabla}\cdot\mathbf{J} &= -p + 2\int d\mathbf{n}'\int d\mathbf{n}_1\int d\mathbf{n}_2\bigg[p + D\, n_i' J_i \\ &\quad + \frac{D+2}{2} n_i'\hat{\sigma}_{ij}n_j'\bigg]\Psi(\mathbf{n}'\rightarrow\mathbf{n}_1,\mathbf{n}_2|\mathbf{N}) \\ &\quad \times\frac{1}{\cos\theta_1 - (\sin\theta_1/\sin\theta_2)\cos\theta_2} \\ &= (k_1-1)p + k_3\frac{D+2}{2}\hat{\sigma}_{NN}. \end{aligned}\tag{A1}$$

Please note that a contribution occurs only from terms which are even with respect to $\mathbf{n}'\rightarrow-\mathbf{n}'$. The first coefficient is given by

$$k_1 = 2\int d\mathbf{n}'\int d\mathbf{n}_1\int d\mathbf{n}_2\Psi(\mathbf{n}'\rightarrow\mathbf{n}_1,\mathbf{n}_2|\mathbf{N}) \times\frac{1}{\cos\theta_1 - (\sin\theta_1/\sin\theta_2)\cos\theta_2}. \tag{A2}$$

The second coefficient k_3 appears when performing a decomposition of the tensor

$$2\int d\mathbf{n}'\int d\mathbf{n}_1\int d\mathbf{n}_2 n_i' n_j'\Psi(\mathbf{n}'\rightarrow\mathbf{n}_1,\mathbf{n}_2|\mathbf{N}) \times\frac{1}{\cos\theta_1 - (\sin\theta_1/\sin\theta_2)\cos\theta_2} = k_3^0\delta_{ij} + k_3 N_i N_j. \tag{A3}$$

The coefficient k_3^0 is irrelevant because $\delta_{ij}\hat{\sigma}_{ij}=0$, where $\hat{\sigma}_{ij}=\sigma_{ij}-\delta_{ij}p$. Then the coefficient k_3 is given by

$$k_3 = 2\int d\mathbf{n}'\int d\mathbf{n}_1\int d\mathbf{n}_2[2(\mathbf{n}'\cdot\mathbf{N})^2-1]\Psi(\mathbf{n}'\rightarrow\mathbf{n}_1,\mathbf{n}_2|\mathbf{N}) \times\frac{1}{\cos\theta_1 - (\sin\theta_1/\sin\theta_2)\cos\theta_2}. \tag{A4}$$

One finally obtains

$$c_1 = k_1 - \frac{D+2}{2}k_3, \quad c_2 = \frac{D+2}{2}k_3. \tag{A5}$$

Explicit expressions for the constants k_1, k_3 are given in Sec. B 4 which finally will have to be evaluated numerically.

2. First moment

Next, let us derive the equation of mechanical equilibrium (114). Taking the first moment of the force density equation without an external force gives

$$\frac{\lambda}{D}\partial_j\sigma_{ij} = -J_i + 2\int d\mathbf{n}'\int d\mathbf{n}_1\int d\mathbf{n}_2 n_{1,i}F(\mathbf{n}',\mathbf{r}) \times\Psi(\mathbf{n}'\rightarrow\mathbf{n}_1,\mathbf{n}_2|\mathbf{N})\frac{1}{\cos\theta_1 - (\sin\theta_1/\sin\theta_2)\cos\theta_2}. \tag{A6}$$

The second term contains the integral

$$\int d\mathbf{n}_1\int d\mathbf{n}_2 n_{1,i}\Psi(\mathbf{n}'\rightarrow\mathbf{n}_1,\mathbf{n}_2|\mathbf{N}) \times\frac{1}{\cos\theta_1 - (\sin\theta_1/\sin\theta_2)\cos\theta_2} = a n_i'. \tag{A7}$$

Symmetrizing the integrand with respect to the indices 1 and 2 gives $a=1/2$. This result is independent of the specific form for the scattering cross section $\Psi(\mathbf{n}'\rightarrow\mathbf{n}_1,\mathbf{n}_2|\mathbf{N})$. The remaining integral with respect to $\mathbf{n}'$ yields J_i canceling the first term $-J_i$ above.

3. Second moment

Finally, we calculate the coefficients B_μ in the third of the continuum equations, Eq. (115). Let us consider the second moment by multiplying the force density equation by $n_{1,i}n_{1,j}$ and integrating with respect to $\mathbf{n}_1$. One obtains the following equation:

$$\lambda D\Gamma_{ijkl}\partial_k J_l = -\frac{1}{D}\sigma_{ij} + \int d\mathbf{n}' F(\mathbf{n}',\mathbf{r})I_{ij}(\mathbf{n}',\mathbf{N}), \tag{A8}$$

where

$$I_{ij}(\mathbf{n}',\mathbf{N})=2\int d\mathbf{n}_1\int d\mathbf{n}_2 n_{1,i}n_{1,j}\Psi(\mathbf{n}'\to\mathbf{n}_1,\mathbf{n}_2|\mathbf{N})\times\frac{1}{\cos\theta_1-(\sin\theta_1/\sin\theta_2)\cos\theta_2} \quad \text{(A9)}$$

and

$$\Gamma_{ijkl}=\frac{1}{D(D+2)}(\delta_{ij}\delta_{kl}+\delta_{ik}\delta_{jl}+\delta_{il}\delta_{jk}). \quad \text{(A10)}$$

The tensor I_{ij} may be decomposed as follows:

$$I_{ij}(\mathbf{n}',\mathbf{N})=K_0\delta_{ij}+K_1 n_i' n_j'+K_2(n_i' N_j+n_j' N_i). \quad \text{(A11)}$$

The coefficients K_0, K_1, and K_2 are all functions of the argument $\mathbf{n}'\cdot\mathbf{N}$ which will be suppressed in the following. As the tensor $I_{ij}(\mathbf{n}',\mathbf{N})$ should be invariant with respect to the operation $\mathbf{N}\to-\mathbf{N}$ because the scattering cross section $\Psi(\mathbf{n}'\to\mathbf{n}_1,\mathbf{n}_2|\mathbf{N})$ is, the functions K_0 and K_1 are even and K_2 is odd under this "parity" change. They are to be determined by multiplying I_{ij} as follows:

$$I_0=I_{ii}=K_0 D+K_1+2K_2(\mathbf{n}'\cdot\mathbf{N}), \quad \text{(A12)}$$

$$I_1=N_i I_{ij} N_j=K_0+K_1(\mathbf{n}'\cdot\mathbf{N})^2+2K_2(\mathbf{n}'\cdot\mathbf{N}), \quad \text{(A13)}$$

$$I_2=n_i' I_{ij} n_j'=K_0+K_1+2K_2(\mathbf{n}'\cdot\mathbf{N}). \quad \text{(A14)}$$

The variables I_0, I_1, and I_2 are likewise functions of the argument $\mathbf{n}'\cdot\mathbf{N}$ which is suppressed henceforth. In the following we consider $D=2$. The system of equations may then be written in matrix form

$$(I_0,I_1,I_2)^T=\mathbf{A}(K_0,K_1,K_2)^T, \quad \text{(A15)}$$

with

$$\mathbf{A}=\begin{pmatrix} 2 & 1 & 2\cos\alpha \\ 1 & \cos^2\alpha & 2\cos\alpha \\ 1 & 1 & 2\cos\alpha \end{pmatrix}, \quad \text{(A16)}$$

where $\cos\alpha=(\mathbf{n}'\cdot\mathbf{N})$. We eventually want the functions K_μ as a function of the integrals I_μ, $\mu=0,1,2$. So we need the inverse matrix

$$\mathbf{A}^{-1}=\begin{pmatrix} 1 & 0 & -1 \\ 0 & 1/\sin^2\alpha & 1/\sin^2\alpha \\ -1/(2\cos\alpha) & 1/(2\cos\alpha\sin^2\alpha) & -\cos(2\alpha)/(2\cos\alpha\sin^2\alpha) \end{pmatrix}. \quad \text{(A17)}$$

We find

$$K_0=I_0-I_2, \quad \text{(A18)}$$

$$K_1=\frac{1}{\sin^2\alpha}(I_2-I_1), \quad \text{(A19)}$$

$$K_2=\frac{1}{2\cos\alpha}\left(-I_0+\frac{1}{\sin^2\alpha}[I_1-\cos(2\alpha)I_2]\right). \quad \text{(A20)}$$

Before writing down the integrals I_μ, let us introduce the vector

$$\mathbf{n}_\perp=\frac{\mathbf{N}-(\mathbf{n}\cdot\mathbf{N})\mathbf{n}}{\sqrt{1-(\mathbf{n}\cdot\mathbf{N})^2}}. \quad \text{(A21)}$$

Furthermore, let us denote the integrals

$$\begin{pmatrix} i_0 \\ i_1 \\ i_2 \end{pmatrix}(\alpha)=2\int d\mathbf{n}_1\int d\mathbf{n}_2\begin{pmatrix} (\mathbf{n}_1\cdot\mathbf{n}')^2 \\ (\mathbf{n}_1\cdot\mathbf{n}'_\perp)^2 \\ (\mathbf{n}_1\cdot\mathbf{n}'_\perp)(\mathbf{n}_1\cdot\mathbf{n}') \end{pmatrix}\times\Psi(\mathbf{n}'\to\mathbf{n}_1,\mathbf{n}_2|\mathbf{N})\times\frac{1}{\cos\theta_1-(\sin\theta_1/\sin\theta_2)\cos\theta_2}. \quad \text{(A22)}$$

Then, we find for the functions K_μ,

$$K_0=i_1, \quad \text{(A23)}$$

$$K_1=-i_1+i_0-2\,\mathrm{sgn}(\sin\alpha)\cot\alpha\, i_2, \quad \text{(A24)}$$

$$K_2=\mathrm{sgn}(\sin\alpha)\frac{i_2}{\sin\alpha}. \quad \text{(A25)}$$

The transformation from I_0,I_1,I_2 to i_0,i_1,i_2 is primarily for technical reasons as in the scattering function the directions $\mathbf{n}_1$ and $\mathbf{n}_2$ are parametrized with respect to $\mathbf{n}'$. We may now proceed to perform the integral on the rhs of Eq. (A8)

$$\int d\mathbf{n}' F(\mathbf{n}',\mathbf{r}) I_{ij}(\mathbf{n}',\mathbf{N}) = \int d\mathbf{n}' \left(p + DJ_k n'_k + \frac{D+2}{2}\hat{\sigma}_{kl} n'_k n'_l \right) I_{ij}(\mathbf{n}',\mathbf{N})$$
$$= p\left(\delta_{ij}\int d\mathbf{n}' K_0 + \int d\mathbf{n}' K_1 n'_i n'_j + \int d\mathbf{n}' K_2 (n'_i N_j + n'_j N_i) \right)$$
$$+ DJ_k \left(\delta_{ij}\int d\mathbf{n}' K_0 n'_k + \int d\mathbf{n}' K_1 n'_i n'_j n'_k + \int d\mathbf{n}' K_2 (n'_i N_j + n'_j N_i) n'_k \right) + \frac{D+2}{2}\hat{\sigma}_{kl}\left(\delta_{ij}\int d\mathbf{n}' K_0 n'_k n'_l + \int d\mathbf{n}' K_1 n'_i n'_j n'_k n'_l \right.$$
$$\left. + \int d\mathbf{n}' K_2 (n'_i N_j + n'_j N_i) n'_k n'_l \right). \tag{A26}$$

The integrals which are multiplied by J_k give no contribution because due to their tensorial properties they should all be linear in **N** which means that they are uneven under sign change **N**. On the other hand, the integrands are even with respect to this operation, which implies that the integrals are zero.

We now further simplify the integrals with respect to $\mathbf{n}'$ multiplied by p and $\hat{\sigma}_{kl}$ using decomposition according to Cartesian tensors. The integrals following p are denoted as follows:

$$\int d\mathbf{n}' K_0 = \overline{K}_0, \tag{A27}$$

$$\int d\mathbf{n}' K_1 n'_i n'_j = \overline{K}_{1,a}\delta_{ij} + \overline{K}_{1,b} N_i N_j, \tag{A28}$$

$$\int d\mathbf{n}' K_2 (n'_i N_j + n'_j N_i) = \overline{K}_{2,a}\delta_{ij} + \overline{K}_{2,b} N_i N_j. \tag{A29}$$

The constants are given by

$$\overline{K}_{1,a} = \int d\alpha K_1 \sin^2\alpha, \tag{A30}$$

$$\overline{K}_{1,b} = \int d\alpha K_1 \cos(2\alpha), \tag{A31}$$

$$\overline{K}_{2,a} = 0, \tag{A32}$$

$$\overline{K}_{2,b} = 2\int d\alpha K_2 \cos\alpha. \tag{A33}$$

The angular integrations above (and all the ones following below) are understood to be normalized by factors $1/(2\pi)$. The integrals following $\hat{\sigma}_{\gamma\delta}$ are the following:

$$\int d\mathbf{n}' K_0 n'_i n'_j = \overline{K}_{0,a}\delta_{ij} + \overline{K}_{0,b} N_i N_j, \tag{A34}$$

$$M_{ijkl} = \int d\mathbf{n}' K_1 n'_i n'_j n'_k n'_l$$
$$= \widetilde{K}_1(\delta_{ij}\delta_{kl} + \delta_{ik}\delta_{jl} + \delta_{il}\delta_{jk}) + \widetilde{K}_2(N_i N_j \delta_{kl} + \text{permutation}) + \widetilde{K}_3 N_i N_j N_k N_l, \tag{A35}$$

and

$$\int d\mathbf{n}' K_2 (n'_i N_j + n'_j N_i) n'_k n'_l$$
$$= \overline{K}'_2 (2N_i N_j \delta_{kl} + N_i N_k \delta_{jl} + N_j N_k \delta_{il} + N_i N_l \delta_{jk} + N_j N_l \delta_{ik}) + 2\overline{K}''_2 N_i N_j N_k N_l. \tag{A36}$$

Let us turn to the first of these three integrals. The coefficients are given by the following integrals:

$$\overline{K}_{0,a} = \int d\alpha K_0 \sin^2\alpha, \tag{A37}$$

$$\overline{K}_{0,b} = \int d\alpha K_0 \cos(2\alpha). \tag{A38}$$

The second integral (A35) giving rise to the coefficients $\widetilde{K}_i$ is treated by performing the following contractions:

$$M_1 = M_{iijj} = \int d\mathbf{n}' K_1, \tag{A39}$$

$$M_2 = M_{iikl} N_k N_l = \int d\alpha K_1 \cos^2\alpha, \tag{A40}$$

$$M_3 = M_{ijkl} N_i N_j N_k N_l = \int d\alpha K_1 \cos^4\alpha. \qquad \text{(A41)}$$

In matrix notation, the system of equations we have to invert is the following:

$$(M_1, M_2, M_3)^T = \mathbf{B}(\tilde{K}_1, \tilde{K}_2, \tilde{K}_3)^T, \qquad \text{(A42)}$$

with

$$\mathbf{B} = \begin{pmatrix} D(D+2) & 2D+4 & 1 \\ D+2 & D+5 & 1 \\ 3 & 6 & 1 \end{pmatrix}. \qquad \text{(A43)}$$

Then, for $D=2$ one finally obtains for the coefficients

$$\tilde{K}_1 = \int d\alpha K_1 \left(\frac{1}{3} - \frac{2}{3}\cos^2\alpha + \frac{1}{3}\cos^4\alpha \right), \qquad \text{(A44)}$$

$$\tilde{K}_2 = \int d\alpha K_1 \left(-\frac{1}{3} + \frac{5}{3}\cos^2\alpha - \frac{4}{3}\cos^4\alpha \right), \qquad \text{(A45)}$$

$$\tilde{K}_3 = \int d\alpha K_1 (1 - 8\cos^2\alpha + 8\cos^4\alpha). \qquad \text{(A46)}$$

Finally, the coefficients of the third integral (A36) read as

$$\overline{K_2'} = \int d\alpha K_2 \cos\alpha \sin^2\alpha, \qquad \text{(A47)}$$

$$\overline{K_2''} = \int d\alpha K_2 \cos\alpha (1 - 4\sin^2\alpha). \qquad \text{(A48)}$$

Next, one collects all coefficients in front of the Cartesian tensors on the rhs of the second moment (A8):

$$\lambda D \Gamma_{ijkl} \nabla_k J_l = -\frac{1}{D}\sigma_{ij} + \hat{\sigma}_{ij}(D+2)\tilde{K}_1 + \delta_{ij}(a_0 p + a_1 \hat{\sigma}_{NN}) + N_i N_j (a_2 p + a_3 \hat{\sigma}_{NN}) + a_4 (N_j \hat{\sigma}_{ik} N_k + N_i \hat{\sigma}_{jk} N_k), \qquad \text{(A49)}$$

where the coefficients a_μ are given as follows:

$$a_0 = \overline{K_0} + \overline{K_{1,a}}, \qquad \text{(A50)}$$

$$a_1 = \frac{D+2}{2}(\overline{K_{0,b}} + \tilde{K}_2), \qquad \text{(A51)}$$

$$a_2 = \overline{K_{1,b}} + \overline{K_{2,b}}, \qquad \text{(A52)}$$

$$a_3 = \frac{D+2}{2}(\tilde{K}_3 + 2\overline{K_2''}), \qquad \text{(A53)}$$

$$a_4 = (D+2)(\tilde{K}_2 + \overline{K_2'}). \qquad \text{(A54)}$$

When reducing the integrals in terms of the integrals i_μ, one obtains

$$a_0 = \int d\alpha [i_0 \sin^2\alpha + i_1 \cos^2\alpha - i_2\, \mathrm{sgn}(\sin\alpha)\sin(2\alpha)], \qquad \text{(A55)}$$

$$a_1 = \frac{D+2}{2}\left(\int d\alpha i_2\, \mathrm{sgn}(\sin\alpha)\cos(2\alpha) + \tilde{K}_2 \right), \qquad \text{(A56)}$$

$$a_2 = \int d\alpha [(i_0 - i_1)\cos(2\alpha) + 2 i_2\, \mathrm{sgn}(\sin\alpha)\sin(2\alpha)], \qquad \text{(A57)}$$

$$a_3 = \frac{D+2}{2}\int d\alpha \{(i_0 - i_1)[1 - 2\sin^2(2\alpha)] + 4 i_2\, \mathrm{sgn}(\sin\alpha)\sin(2\alpha)\cos(2\alpha)\}, \qquad \text{(A58)}$$

$$a_4 = (D+2)\left[\tilde{K}_2 + \frac{1}{2}\int d\alpha i_2\, \mathrm{sgn}(\sin\alpha)\sin(2\alpha) \right], \qquad \text{(A59)}$$

and

$$\tilde{K}_1 = \int d\alpha [(i_0 - i_1)\sin\alpha - 2 i_2\, \mathrm{sgn}(\sin\alpha)\cos\alpha] \times \frac{\sin\alpha}{3}(-1 + 4\cos^2\alpha), \qquad \text{(A60)}$$

where

$$\tilde{K}_2 = \int d\alpha [(i_0 - i_1)\sin\alpha - 2 i_2\, \mathrm{sgn}(\sin\alpha)\cos\alpha] \times \frac{\sin\alpha}{3}(-1 + 4\cos^2\alpha). \qquad \text{(A61)}$$

Using the equation for the zeroth moment (113), we can eliminate p and we obtain the coefficients B_0 through B_5,

$$B_0 = -\frac{1}{D} + (D+2)\tilde{K}_1, \qquad \text{(A62)}$$

$$B_1 = \frac{1}{(c_1 - 1)}[a_0 - a_1 - (D+2)\tilde{K}_1], \qquad \text{(A63)}$$

$$B_2 = a_1 + \frac{c_2}{c_1 - 1}[-a_0 + a_1 + (D+2)\tilde{K}_1], \qquad \text{(A64)}$$

$$B_3 = \frac{1}{c_1 - 1}(a_2 - a_3 - 2a_4), \qquad \text{(A65)}$$

$$B_4 = a_3 + \frac{c_2}{c_1 - 1}(-a_2 + a_3 + 2a_4), \qquad \text{(A66)}$$

$$B_5 = a_4. \qquad \text{(A67)}$$

Inserting for c_1, c_2 calculated in Sec. B 1, and for $\tilde{K}_1$, $\tilde{K}_2$, and a_0 through a_4 given above, the coefficients B_μ are en-

TABLE I. The microscopic constants c_0, c_1, and B_μ, $\mu=0,\ldots,5$, and the entries a,b,c,c',d of the matrix $\Lambda_\dagger$ calculated from the microscopic model for scattering for different bias intensities p, where the maximum scattering angle is $\theta_{max}=\pi/2-0.01$.

p	0	1	2	4	6	8
c_1-1	3.23966	5.98386	6.91022	7.66596	8.00018	8.19206
c_2	$<10^{-9}$	-2.73543	-3.6542	-4.39914	-4.72539	-4.91083
B_0	-2.02254	-3.07827	-3.49472	-3.87001	-4.04823	-4.15404
B_1	1.12431	1.05801	1.03896	1.02225	1.01434	1.00966
B_2	$<10^{-9}$	0.478234	0.688084	0.897999	1.00432	1.06907
B_3	$<10^{-9}$	-0.0871608	-0.0664648	-0.0348425	-0.0166413	-0.00515556
B_4	$<10^{-9}$	-0.248513	-0.968517	-1.88383	-2.39835	-2.72395
B_5	$<10^{-9}$	1.05321	1.64421	2.26475	2.58598	2.7831
a	0.185067	0.250961	0.374958	0.594681	0.751558	0.862493
b	0.185067	0.297586	0.45714	0.727492	0.916382	1.04853
c	0.432281	0.308721	0.315767	0.368355	0.416152	0.452717
c'	0.432281	0.971317	1.48443	2.25966	2.76618	3.10848
d	-0.247214	-0.246906	-0.270197	-0.311477	-0.341938	-0.364713
r	1.0	0.914026	0.438156	-0.042155	-0.260547	-0.383077
t	1.0	0.843324	0.820227	0.81744	0.820136	0.822574

tirely determined in terms of integrals over the scattering function or in terms of integrals over the functions i_μ which have to be evaluated numerically. Explicit expressions for the functions i_μ for a specific scattering model are given in Sec. B 4 and have been used to yield the following Tables I–IV.

4. The scattering model

We give now the explicit form for the normalization factor C_p of the microscopic scattering model, Eq. (130). Choosing the angle between $\mathbf{n}'$ and $\mathbf{N}$ as α one finds the following relation to determine C_p:

$$1=\int d\mathbf{n}_1\int d\mathbf{n}_2\Psi(\mathbf{n}'\to\mathbf{n}_1,\mathbf{n}_2|\mathbf{N})$$

$$=C_p 2\int_0^{\theta_{max}}\frac{d\theta_1}{\theta_{max}}\int_{-\theta_{max}}^{-\theta_1}\frac{d\theta_2}{(\theta_{max}-\theta_1)}\times[\cos^{2p}(\theta_1-\alpha)+\cos^{2p}(\theta_1+\alpha)]. \tag{A68}$$

One finds

TABLE II. The microscopic constants c_0, c_1, and B_μ, $\mu=0,\ldots,5$, and the entries a,b,c,c',d of the matrix $\Lambda_\dagger$ calculated from the microscopic model for scattering for different bias intensities p, where the maximum scattering angle is $\theta_{max}=\pi/2-0.05$.

p	0	1	2	4	6	8
c_1-1	1.90263	3.3809	3.90443	4.36006	4.57993	4.7162
c_2	$<10^{-9}$	-1.4544	-1.95725	-2.38459	-2.58451	-2.70519
B_0	-1.34045	-1.97435	-2.22524	-2.45813	-2.57493	-2.64818
B_1	1.20453	1.12804	1.10869	1.09218	1.08417	1.0792
B_2	$<10^{-9}$	0.302278	0.418453	0.53197	0.590517	0.627352
B_3	$<10^{-9}$	-0.0881382	-0.0775209	-0.0563067	-0.0438889	-0.0353852
B_4	$<10^{-9}$	-0.158535	-0.486841	-0.90403	-1.14793	-1.30717
B_5	$<10^{-9}$	0.626319	0.940457	1.26503	1.43651	1.54521
a	0.339085	0.40072	0.51712	0.705856	0.828683	0.915888
b	0.339085	0.501589	0.681264	0.952482	1.1194	1.23675
c	0.712094	0.521519	0.513996	0.548739	0.580671	0.606106
c'	0.712094	1.36669	1.89275	2.61839	3.04756	3.3414
d	-0.373009	-0.370911	-0.38917	-0.419075	-0.439207	-0.453324
r	1.0	0.868488	0.57427	0.252696	0.0920036	-0.00397738
t	1.0	0.7989	0.75906	0.74107	0.740293	0.740561

TABLE III. The microscopic constants c_0, c_1, and B_μ, $\mu=0,\ldots,5$, and the entries a,b,c,c',d of the matrix $\Lambda_\dagger$ calculated from the microscopic model for scattering for different bias intensities p, where the maximum scattering angle is $\theta_{max}=\pi/4$.

p	0	1	2	4	6	8
c_1-1	0.154395	0.224047	0.271432	0.32539	0.355728	0.37555
c_2	$<10^{-9}$	-0.0528349	-0.0821605	-0.113501	-0.130596	-0.14166
B_0	-0.199655	-0.267729	-0.311707	0.360256	-0.386527	-0.403233
B_1	1.79315	1.70859	1.69527	1.68785	1.68312	1.67972
B_2	$<10^{-9}$	0.0282278	0.0350513	0.0396921	0.0413126	0.0421027
B_3	$<10^{-9}$	-0.0272506	-0.0938402	-0.16046	-0.192802	-0.211874
B_4	$<10^{-9}$	-0.0482741	-0.0321304	0.000361819	0.0226003	0.038231
B_5	$<10^{-9}$	0.0590451	0.0753626	0.0858452	0.0893064	0.0908931
a	5.22475	4.46981	3.99399	3.55095	3.33471	3.20677
b	5.22475	5.48863	5.38669	5.23452	5.14104	5.08701
c	7.72907	6.02669	5.24234	4.56791	4.25716	4.07678
c'	7.72907	8.43526	8.55002	8.60126	8.61323	8.63027
d	-2.50432	-2.39596	-2.11555	-1.82208	-1.68225	-1.60082
r	1.0	0.682741	0.765062	0.912647	1.00577	1.06836
t	1.0	0.814376	0.741456	0.678371	0.648644	0.630384

$$C_p(\alpha)=\frac{1}{4}\left[\frac{1}{2^{2p}}\binom{2p}{p}+\frac{2}{\theta_{max}2^{2p}}\sum_{k=0}^{p-1}\binom{2p}{k}\times\frac{\sin[(2p-2k)\theta_{max}]\cos[(2p-2k)\alpha]}{[2(p-k)]}\right]^{-1}. \tag{A69}$$

We have mentioned above that all constants of the continuum equations depend on the parameters k_1, k_3, and the integrals of the functions $i_\mu(\alpha)$ for $\mu=0,1,2$. Using the model for the scattering cross section introduced in the main text, they read as follows:

$$\begin{pmatrix}k_1\\k_3\end{pmatrix}=2\int_{-\pi}^{\pi}\frac{d\alpha}{(2\pi)}C_p(\alpha)\begin{pmatrix}1\\\cos(2\alpha)\end{pmatrix}\times\int_0^{\theta_{max}}\frac{d\theta_1}{\theta_{max}}\int_{-\theta_{max}}^{-\theta_1}\frac{d\theta_2}{(\theta_{max}-\theta_1)}\times\frac{[\cos^{2p}(\theta_1-\alpha)+\cos^{2p}(\theta_1+\alpha)]}{(\cos\theta_1\sin\theta_2-\sin\theta_1\cos\theta_2)}(\sin\theta_2-\sin\theta_1) \tag{A70}$$

and

$$\begin{pmatrix}i_0\\i_1\\i_2\end{pmatrix}(\alpha)=2C_p(\alpha)\int_0^{\theta_{max}}\frac{d\theta_1}{\theta_{max}}\int_{-\theta_{max}}^{-\theta_1}\frac{d\theta_2}{(\theta_{max}-\theta_1)}\times\frac{[\cos^{2p}(\theta_1-\alpha)\pm\cos^{2p}(\theta_1+\alpha)]}{(\cos\theta_1\sin\theta_2-\sin\theta_1\cos\theta_2)}\times\begin{pmatrix}\sin\theta_2\cos^2\theta_1-\sin\theta_1\cos^2\theta_2\\\sin\theta_1\sin\theta_2(\sin\theta_1-\sin\theta_2)\\\sin\theta_1\sin\theta_2(\cos\theta_1-\cos\theta_2)\end{pmatrix}. \tag{A71}$$

The choice of signs indicated on the rhs is to be understood as follows. The $+$ sign is used for i_0, i_1, and the $-$ sign for i_2. Using these expression all constants c_1, c_2, and B_0 through B_5 can be determined.

5. Numerical values of the different coefficients

Microscopic constants c_0, c_1, B_μ, and the entries a,b,c,c',d of the matrix $\Lambda_\dagger$ calculated from the microscopic model for various scattering angles are given in Tables I–IV.

APPENDIX B: RESPONSE FUNCTIONS

1. Region I

The σ_{ij} can be expressed as

$$\sigma_{zz}=\int_0^{+\infty}dq[a_3^*e^{-iqx}+a_4e^{iqx}]e^{iX_4qz}+\int_0^{+\infty}dq[a_4^*e^{-iqx}+a_3e^{iqx}]e^{iX_3qz}, \tag{B1}$$

$$\sigma_{xx}=\int_0^{+\infty}dq[(X_3^2a_3)^*e^{-iqx}+X_4^2a_4e^{iqx}]e^{iX_4qz}+\int_0^{+\infty}dq[(X_4^2a_4)^*e^{-iqx}+X_3^2a_3e^{iqx}]e^{iX_3qz}, \tag{B2}$$

$$\sigma_{xz}=-\int_0^{+\infty}dq[(X_3a_3)^*e^{-iqx}+X_4a_4e^{iqx}]e^{iX_4qz}-\int_0^{+\infty}dq[(X_4a_4)^*e^{-iqx}+X_3a_3e^{iqx}]e^{iX_3qz}. \tag{B3}$$

TABLE IV. The microscopic constants c_0, c_1, and B_μ, $\mu=0,\ldots,5$, and the entries a,b,c,c',d of the matrix $\Lambda_\dagger$ calculated from the microscopic model for scattering for different bias intensities p, where the maximum scattering angle is $\theta_{max}=\pi/8$.

p	0	1	2	4	6	8
c_1-1	0.0335067	0.0428648	0.0524673	0.0641093	0.0705982	0.0747538
c_2	$<10^{-9}$	-0.00668779	-0.0121806	-0.018075	-0.020776	-0.0221954
B_0	-0.0485058	-0.0601859	-0.0709311	-0.0839805	-0.0912928	-0.0959171
B_1	1.94764	1.89848	1.86723	1.86271	1.86831	1.87199
B_2	$<10^{-9}$	0.00497716	0.00718661	0.00839984	0.00836975	0.00806044
B_3	$<10^{-9}$	0.0189319	-0.0293591	-0.104785	-0.149741	-0.177526
B_4	$<10^{-9}$	-0.0118706	-0.0131302	-0.00748694	-0.000990488	0.00438443
B_5	$<10^{-9}$	0.010374	0.0158534	0.0190278	0.0189925	0.018225
a	24.6907	22.0583	19.3127	16.6004	15.1812	14.279
b	24.6907	25.1971	24.085	22.3923	21.0886	20.0854
c	34.9988	29.4735	25.2402	21.4431	19.66	18.5982
c'	34.9988	35.9891	35.1548	33.5005	31.975	30.7187
d	-10.308	-10.0378	-9.07808	-7.69791	-6.91559	-6.43566
r	1.0	0.697308	0.677047	0.784092	0.890948	0.973368
t	1.0	0.87543	0.801857	0.741342	0.719877	0.710911

The top conditions (32) and (33) allow to calculate the coefficients a_3 and a_4. They read

$$a_3=\frac{1}{X_4-X_3}\frac{F_0}{2\pi}(X_4\cos\theta_0+\sin\theta_0), \tag{B4}$$

$$a_4=\frac{1}{X_3-X_4}\frac{F_0}{2\pi}(X_3\cos\theta_0+\sin\theta_0). \tag{B5}$$

To perform the integrals over q, it is useful to define the two following integrals:

$$I_\pm\equiv\int_0^{+\infty}dq\,\cos(qx)e^{-\alpha qz\pm i\beta qz}=\frac{\alpha z\mp i\beta z}{(\alpha z\mp i\beta z)^2+x^2}, \tag{B6}$$

$$J_\pm\equiv\int_0^{+\infty}dq\,\sin(qx)e^{-\alpha qz\pm i\beta qz}=\frac{x}{(\alpha z\mp i\beta z)^2+x^2}. \tag{B7}$$

We then get

$$\sigma_{zz}=\frac{F_0}{2\pi}\frac{4}{2\beta}\left[\beta\cos\theta_0\frac{I_++I_-}{2}+\alpha\cos\theta_0\frac{I_+-I_-}{2i}+\sin\theta_0\frac{J_+-J_-}{2i}\right], \tag{B8}$$

$$\sigma_{xx}=\frac{F_0}{2\pi}\frac{4}{2\beta}\left[\beta(\alpha^2+\beta^2)\cos\theta_0\frac{I_++I_-}{2}-\alpha(\alpha^2+\beta^2)\times\cos\theta_0\frac{I_+-I_-}{2i}-(\alpha^2-\beta^2)\sin\theta_0\frac{J_+-J_-}{2i}+2\alpha\beta\sin\theta_0\frac{J_++J_-}{2}\right], \tag{B9}$$

$$\sigma_{xz}=\frac{F_0}{2\pi}\frac{4}{2\beta}\left[(\alpha^2+\beta^2)\cos\theta_0\frac{J_+-J_-}{2i}+\beta\sin\theta_0\frac{I_++I_-}{2}-\alpha\sin\theta_0\frac{I_+-I_-}{2i}\right]. \tag{B10}$$

2. Region II

The σ_{ij} can be expressed as

$$\sigma_{zz}=\int_0^{+\infty}dq[a_4^*e^{-iqx}+a_4e^{iqx}]e^{iX_4qz}+\int_0^{+\infty}dq[a_3^*e^{-iqx}+a_3e^{iqx}]e^{iX_3qz}, \tag{B11}$$

$$\sigma_{xx}=\int_0^{+\infty}dq[(X_4^2a_4)^*e^{-iqx}+X_4^2a_4e^{iqx}]e^{iX_4qz}+\int_0^{+\infty}dq[(X_3^2a_3)^*e^{-iqx}+X_3^2a_3e^{iqx}]e^{iX_3qz}, \tag{B12}$$

$$\sigma_{xz}=-\int_0^{+\infty}dq[(X_4a_4)^*e^{-iqx}+X_4a_4e^{iqx}]e^{iX_4qz}-\int_0^{+\infty}dq[(X_3a_3)^*e^{-iqx}+X_3a_3e^{iqx}]e^{iX_3qz}. \tag{B13}$$

The top conditions (32) and (33) give again

$$a_3=\frac{1}{X_4-X_3}\frac{F_0}{2\pi}(X_4\cos\theta_0+\sin\theta_0), \tag{B14}$$

$$a_4 = \frac{1}{X_3 - X_4}\frac{F_0}{2\pi}(X_3 \cos\theta_0 + \sin\theta_0). \tag{B15}$$

In this case, the useful integrals are

$$I(\alpha) \equiv \int_0^{+\infty} dq\, \cos(qx) e^{-\alpha q z} = \frac{\alpha z}{(\alpha z)^2 + x^2}, \tag{B16}$$

$$J(\alpha) \equiv \int_0^{+\infty} dq\, \sin(qx) e^{-\alpha q z} = \frac{x}{(\alpha z)^2 + x^2}. \tag{B17}$$

We then get

$$\sigma_{zz} = \frac{F_0}{2\pi}\frac{2}{\alpha_2 - \alpha_1}[\alpha_2 \cos\theta_0 I(\alpha_1) + \sin\theta_0 J(\alpha_1) - \alpha_1 \cos\theta_0 I(\alpha_2) - \sin\theta_0 J(\alpha_2)], \tag{B18}$$

$$\sigma_{xx} = \frac{F_0}{2\pi}\frac{2}{\alpha_2 - \alpha_1}[-\alpha_1^2\alpha_2 \cos\theta_0 I(\alpha_1) - \alpha_1^2 \sin\theta_0 J(\alpha_1) + \alpha_2^2\alpha_1 \cos\theta_0 I(\alpha_2) + \alpha_2^2 \sin\theta_0 J(\alpha_2)], \tag{B19}$$

$$\sigma_{xz} = \frac{F_0}{2\pi}\frac{2}{\alpha_2 - \alpha_1}[\alpha_1\alpha_2 \cos\theta_0 J(\alpha_1) - \alpha_1 \sin\theta_0 I(\alpha_1) - \alpha_2\alpha_1 \cos\theta_0 J(\alpha_2) + \alpha_2 \sin\theta_0 I(\alpha_2)]. \tag{B20}$$

[1] P.-G. de Gennes, Physica A **261**, 293 (1998).
[2] S.B. Savage, in *Physics of Dry Granular Media*, Vol. 25 of *NATO Advanced Studies Institute, Series E: Applied Sciences*, edited by H.J. Herrmann, J.P. Hovi, and S. Luding (Kluwer, Dordrecht, 1997).
[3] J.-P. Bouchaud, P. Claudin, M.E. Cates, and J.P. Wittmer, in *Physics of Dry Granular Media*, Vol. 97 of *NATO Advanced Studies Institute, Series E: Applied Sciences*, edited by H.J. Herrmann, J.P. Hovi, and S. Luding, (Kluwer, Dordrecht, 1997).
[4] M.E. Cates, J.P. Wittmer, J.-P. Bouchaud, and P. Claudin, Philos. Trans. R. Soc. London, Ser. A **356**, 2535 (1998).
[5] F. Cantelaube and J. Goddard, in *Physics of Dry Granular Media*, Vol. 123 of *NATO Advanced Studies Institute, Series E: Applied Sciences*, edited by H.J. Herrmann, J.P. Hovi, and S. Luding (Kluwer, Dordrecht, 1997).
[6] P. Claudin, J.-P. Bouchaud, M.E. Cates, and J.P. Wittmer, Phys. Rev. E **57**, 4441 (1998).
[7] J.-P. Bouchaud, M.E. Cates, and P. Claudin, J. Phys. I **5**, 639 (1995).
[8] S. Ouaguenouni and J.N. Roux, Europhys. Lett. **32**, 449 (1995); **39**, 117 (1997).
[9] C. Moukarzel, Phys. Rev. Lett. **81**, 1634 (1998).
[10] V. Tkachenko and T.A. Witten, Phys. Rev. E **60**, 687 (1999).
[11] S.F. Edwards and D.V. Grinev, Phys. Rev. Lett. **82**, 5397 (1999); S.F. Edwards and D. Grinev, Physica A **294**, 57 (2001).
[12] R.C. Ball and R. Blumenfeld, Phys. Rev. Lett. **88**, 115505 (2002).
[13] J.P. Bouchaud, P. Claudin, D. Levine, and M. Otto, Eur. Phys. J. E **4**, 451 (2001).
[14] J.E.S. Socolar, D.G. Schaeffer, and P. Claudin, Eur. Phys. J. E **7**, 353 (2002); **8**, 453(E) (2002).
[15] E. Clément, G. Reydellet, L. Vanel, D.W. Howell, J. Geng, and R.P. Behringer, in *XIIIth International Congress on Rheology, Cambridge*, edited by D.M. Binding *et al.* (British Society of Rheology, Glasgow, 2000), Vol. 2, p. 426.
[16] G. Reydellet and E. Clément, Phys. Rev. Lett. **86**, 3308 (2001).
[17] D. Serero, G. Reydellet, P. Claudin, E. Clément, and D. Levine, Eur. Phys. J. E **6**, 169 (2001).
[18] C. Goldenberg and I. Goldhirsch, Phys. Rev. Lett. **89**, 084302 (2002).
[19] C. Gay and R. da Silveira, e-print cond-mat/0208155; R. da Silveira, G. Vidalenc, and C. Gay, e-print cond-mat/0208214.
[20] J.P. Wittmer, A. Tanguy, J.-L. Barrat, and L. Lewis, Europhys. Lett. **57**, 423 (2002); A. Tanguy, J.P. Wittmer, F. Leonforte, and J.-L. Barrat, Phys. Rev. B **66**, 174205 (2002).
[21] L. Landau and E. Lifshitz, *Elasticity Theory* (Pergamon, New York, 1986).
[22] C. Truesdell and W. Noll, in *Handbuch der Physik*, edited by S. Flügge and C. Truesdell (Springer, Berlin, 1965), Vol. III/3, pp. 1–579.
[23] C. Fichera, in *Handbuch der Physik*, edited by S. Flügge and C. Truesdell (Springer, Berlin, 1972), Vol. VI a/2, p. 391.
[24] A.E. Green and G.I. Taylor, Proc. R. Soc. London, Ser. A **173**, 162 (1939); **173**, 173 (1939).
[25] L. Breton, P. Claudin, E. Clément, and J.-D. Zucker, Europhys. Lett. **60**, 813 (2002).
[26] J.P. Wittmer, P. Claudin, M.E. Cates, and J.-P. Bouchaud, Nature (London) **382**, 336 (1996); J.P. Wittmer, P. Claudin, M.E. Cates, J. Phys. I **7**, 39 (1997).
[27] J. Geng, R. Reydellet, E. Clément, and R. P. Behringer, Physica D (to be published), e-print cond-mat/0211031.
[28] E. Clément, R. Reydellet, B. Behringer, and J. Geng (private communication); Guillaume Reydellet, Ph.D. thesis, Université Pierre et Marie Curie, Paris, 2002 (unpublished).
[29] J.E.S. Socolar, Discrete Contin Dyn. Syst. Ser. B (to be published).
[30] An alternative definition of $P(f,\mathbf{n},\mathbf{r})$ such that $P(f,\mathbf{n},\mathbf{r}) \sim f^{-D}$ is used in Ref. [29] which makes invariance of the full nonlinear model with respect to rescaling of all force intensities most transparent. For the present work where mergings of force chains are neglected, this aspect is not relevant.
[31] M.C.W. van Rossum and Th.M. Nieuwenhuizen, Rev. Mod. Phys. **71**, 313 (1999).
[32] J.P. Bouchaud, P. Claudin, M. Otto, and J.E.S. Socolar (unpublished).
[33] J. Garnier, Ph.D. thesis, Université de Grenoble, 1973 (unpublished).